Computer Physics Communications 287 (2023) 108689

Contents lists available at ScienceDirect

Computer Physics Communications

journal homepage: www.elsevier.com/locate/cpc

Implementation of the quasiparticle finite amplitude method within the relativistic self-consistent mean-field framework (II): The program DIRQFAM v2.0.0 ☆,☆☆

A. Bjelčić, T. Nikšić *

University of Zagreb, Faculty of Science, Physics Department, Croatia

ARTICLE INFO

Article history:
Received 15 September 2022
Received in revised form 3 January 2023
Accepted 31 January 2023
Available online 9 February 2023

Keywords:
Relativistic quasiparticle random-phase approximation
Finite amplitude method
Multipole response
Dirac-Hartree-Bogoliubov
Nuclear energy density functional

ABSTRACT

We describe the new version 2.0.0 of the code DIRQFAM that calculates the multipole response of even-even axially symmetric deformed nuclei using the framework of relativistic self-consistent mean-field models. The response is calculated by implementing the finite amplitude method for relativistic quasiparticle random phase approximation. In the new version, we have implemented the following features: (i) meson-exchange interactions, (ii) low-rank method for calculating induced densities and currents, (iii) generalized minimal residual method (GMRES), (iv) evaluation of the nucleon localization function, (v) extraction of the QRPA transition matrix elements and eigenfrequencies, (vi) evaluation of the H^{11} part of the induced Hamiltonian, (vii) multipole excitation operators up to $J \leq 5$ are now included.

Program summary
Program title: DIRQFAM v2.0.0
CPC Library link to program files: https://doi.org/10.17632/6gv8nxg4ns.2
Licensing provisions: GPLv3
Programming language: Fortran 90.
External routines/libraries: BLAS/LAPACK, version 3.1. or higher.
Journal reference of previous version: A. Bjelčić, T. Nikšić, Comp. Phys. Comm. 253, 107184 (2020).
Does the new version supersede the previous version?: Yes
Nature of problem: Multipole response of deformed even-even open-shell nuclei can be calculated using the quasiparticle finite amplitude method (QFAM), based on the relativistic self-consistent mean-field models. The particle-hole channel is described by a zero-range relativistic effective interaction or interaction based on meson exchange, while the particle-particle channel of the effective inter-nucleon interaction is described by a separable finite-range pairing force. The method can be applied to perform systematic studies of collective modes even in heavy deformed nuclei.
Solution method: The current implementation computes the multipole response by solving the QFAM equations in a self-consistent iteration scheme. At each iteration the QFAM solutions are updated using the GMRES method. The QFAM amplitudes are expanded in the simplex-y harmonic oscillator basis.
Summary of revisions:

1. meson-exchange interaction are included in the code;
2. calculation of the nucleon localization function;
3. extraction of the QRPA transition matrix elements and eigenfrequencies;
4. evaluation of the H^{11} part of the induced Hamiltonian;
5. multipoles excitation operators up to $J \leq 5$ are included;
6. low-rank method for calculating induced densities and currents;
7. generalized minimal residual method;
8. dynamic memory allocation;

☆ The review of this paper was arranged by Prof. Z. Was.
☆☆ This paper and its associated computer program are available via the Computer Physics Communications homepage on ScienceDirect (http://www.sciencedirect.com/science/journal/00104655).

* Corresponding author.
E-mail address: tniksic@phy.hr (T. Nikšić).

https://doi.org/10.1016/j.cpc.2023.108689

9. reduced memory requirements;

Additional comments including restrictions and unusual features: Open-shell even-even nuclei with parity conserved axially symmetric ground states are considered. An electric multipole operator with $J \leq 5$ is used to calculate the response function.

1. Introduction

In Ref. [1] we have presented the DIRQFAM computer code to calculate the multipole response of even-even axially symmetric deformed nuclei using the framework of relativistic self-consistent mean-field models. The response is calculated by implementing the quasiparticle finite amplitude method (QFAM) for relativistic quasiparticle random phase approximation (QRPA). The present paper is a long write-up of the new version of the DIRQFAM code with a number of new features such as meson-exchange interactions, implementation of the low-rank method for calculating induced densities and currents, generalized minimal residual method (GMRES) instead of the Broyden's mixing method, calculation of the nucleon localization function, extraction of the QRPA transition matrix elements and eigenfrequencies and calculation of the H^{11} part of the induced Hamiltonian, multipole excitation operators up to $J \leq 5$. Furthermore, dynamic memory allocation is used instead of the static memory allocation and the memory requirements are reduced. Unless stated otherwise, details about the methods presented in Ref. [1] are still applicable.

The paper is organized as follows. In Sec. 2, we present the modifications introduced in this version of the code. In. Sec. 3, we describe the new options available in the input file and explain how to run the code. Short summary is given in Sec. 4 and further mathematical details can be found in appendices.

2. Modifications introduced in version 2.0.0

2.1. Meson-exchange models

The meson-exchange model is defined by the Lagrangian density:

$$\mathcal{L} = \mathcal{L}_N + \mathcal{L}_m + \mathcal{L}_{int}. \tag{1}$$

$\mathcal{L}_N$ denotes the Lagrangian of the free nucleon:

$$\mathcal{L}_N = \bar{\psi}(\mathrm{i}\gamma^\mu \partial_\mu - m)\psi, \tag{2}$$

where m is the bare nucleon mass and ψ denotes the Dirac spinor. $\mathcal{L}_m$ is the Lagrangian for the free meson fields and electromagnetic field:

$$\begin{aligned}\mathcal{L}_m = &\frac{1}{2}\partial_\mu\sigma\,\partial^\mu\sigma - \frac{1}{2}m_\sigma^2\sigma^2 - \frac{1}{4}\Omega_{\mu\nu}\Omega^{\mu\nu} + \frac{1}{2}m_\omega^2\omega_\mu\omega^\mu \\ &- \frac{1}{4}\vec{R}_{\mu\nu}\cdot\vec{R}^{\mu\nu} + \frac{1}{2}m_\rho^2\vec{\rho}_\mu\cdot\vec{\rho}^\mu - \frac{1}{4}F_{\mu\nu}F^{\mu\nu},\end{aligned} \tag{3}$$

with the corresponding masses m_σ, m_ω, m_ρ, and $\Omega_{\mu\nu}$, $\vec{R}_{\mu\nu}$, $F_{\mu\nu}$ are field tensors:

$$\Omega^{\mu\nu} = \partial^\mu\omega^\nu - \partial^\nu\omega^\mu, \tag{4}$$

$$\vec{R}^{\mu\nu} = \partial^\mu\vec{\rho}^\nu - \partial^\nu\vec{\rho}^\mu, \tag{5}$$

$$F^{\mu\nu} = \partial^\mu A^\nu - \partial^\nu A^\mu. \tag{6}$$

Arrows denote isovectors and boldface symbols are used for vectors in ordinary space. The minimal set of interaction terms is contained in $\mathcal{L}_{int}$:

$$\mathcal{L}_{int} = -g_\sigma\bar{\psi}\psi\sigma - g_\omega\bar{\psi}\gamma^\mu\psi\omega_\mu - g_\rho\bar{\psi}\vec{\tau}\gamma^\mu\psi\cdot\vec{\rho}_\mu - e\frac{1+\tau_3}{2}\bar{\psi}\gamma^\mu\psi A_\mu, \tag{7}$$

with the couplings g_σ, g_ω, g_ρ and e.

From the Lagrangian density, one can easily obtain the Hamiltonian density $\mathcal{H}(\boldsymbol{r})$ (for details see Ref. [2] and references cited therein). We also introduce the isoscalar-scalar density, the isoscalar-vector current, the isovector-vector current and the proton current:

$$\rho_s(\boldsymbol{r}) = \sum_{i=1}^{A}\bar{\psi}_i(\boldsymbol{r})\psi_i(\boldsymbol{r}), \tag{8}$$

$$j^\mu(\boldsymbol{r}) = \sum_{i=1}^{A}\bar{\psi}_i(\boldsymbol{r})\gamma^\mu\psi_i(\boldsymbol{r}), \tag{9}$$

$$\vec{j}^\mu(\boldsymbol{r}) = \sum_{i=1}^{A}\bar{\psi}_i(\boldsymbol{r})\vec{\tau}\gamma^\mu\psi_i(\boldsymbol{r}), \tag{10}$$

$$j_p^{\mu}(\boldsymbol{r}) = \sum_{i=1}^{Z} \psi_i^{\dagger}(\boldsymbol{r}) \gamma^{\mu} \psi_i(\boldsymbol{r}), \tag{11}$$

where the summation is performed only over occupied orbits in the Fermi sea of positive energy states, i.e. the *no-sea* approximation is used. By integrating the Hamiltonian density we obtain the total energy which depends on the Dirac spinors and the meson fields:

$$E_{RMF}[\psi, \bar{\psi}, \sigma, \omega^{\mu}, \vec{\rho}^{\mu}, A^{\mu}] = \int d\boldsymbol{r}\, \mathcal{H}(\boldsymbol{r}). \tag{12}$$

The meson-nucleon couplings $g_{\sigma}(\rho_v)$, $g_{\omega}(\rho_v)$ and $g_{\rho}(\rho_v)$ are assumed to be functions of the vector density $\rho_v = j^0$. The density-dependence of the couplings is described by a phenomenological ansatz with parameters adjusted to the experimental data in finite nuclei [3–6].

The single-nucleon Dirac equation is derived by variation of the energy density functional (12) with respect to $\bar{\psi}$:

$$\hat{h}_D \psi_i = \epsilon_i \psi_i, \tag{13}$$

with the Dirac Hamiltonian:

$$\hat{h}_D = \begin{bmatrix} \Sigma^0 + \Sigma_R^0 + (\Sigma_s + m) & \boldsymbol{\sigma} \cdot (\boldsymbol{p} - \boldsymbol{\Sigma}), \\ \boldsymbol{\sigma} \cdot (\boldsymbol{p} - \boldsymbol{\Sigma}) & \Sigma^0 + \Sigma_R^0 - (\Sigma_s + m) \end{bmatrix}. \tag{14}$$

The nucleon self-energies are defined by the following expressions:

$$\begin{aligned} \Sigma_s &= g_{\sigma}(\rho_v)\sigma, \\ \Sigma^{\mu} &= g_{\omega}(\rho_v)\omega^{\mu} + g_{\rho}(\rho_v)\vec{\tau} \cdot \vec{\rho}^{\mu} + e\frac{1+\tau_3}{2}A^{\mu}, \\ \Sigma_R^0 &= g'_{\sigma}(\rho_v)\rho_s\sigma + g'_{\omega}(\rho_v)\rho_v\omega^0 + g'_{\rho}(\rho_v)\vec{j}^0 \cdot \vec{\rho}^0. \end{aligned} \tag{15}$$

The last *rearrangement* contribution Σ_R^0 is a consequence of density dependence of the vertex functions $g_{\sigma}(\rho_v)$, $g_{\omega}(\rho_v)$, and $g_{\rho}(\rho_v)$. The variation of the energy density functional (12) with respect to the meson fields leads to the Helmholtz equations for the meson fields:

$$\left[-\triangle + m_{\sigma}^2\right]\sigma = -g_{\sigma}(\rho_v)\rho_s, \tag{16}$$

$$\left[-\triangle + m_{\omega}^2\right]\omega^{\mu} = g_{\omega}(\rho_v) j^{\mu}, \tag{17}$$

$$\left[-\triangle + m_{\rho}^2\right]\vec{\rho}^{\mu} = g_{\rho}(\rho_v)\vec{j}^{\mu}, \tag{18}$$

and to the Poisson equation for the electromagnetic field:

$$-\triangle A^{\mu} = e j_p^{\mu}. \tag{19}$$

Because of charge conservation, only the third component of the isovector ρ-meson contributes. In the ground-state solution for an even-even nucleus there are no currents (time-reversal invariance), and the corresponding spatial components of the meson-fields vanish $\boldsymbol{\Sigma} = 0$. The Dirac equation takes a simple form that includes only the vector potential $V(\boldsymbol{r})$ and the effective mass $M^*(\boldsymbol{r}) = m + g_{\sigma}(\rho_v)\sigma$:

$$\{-\mathrm{i}\boldsymbol{\alpha} \cdot \boldsymbol{\nabla} + \beta M^*(\boldsymbol{r}) + V(\boldsymbol{r})\}\psi_i(\boldsymbol{r}) = \epsilon_i \psi_i(\boldsymbol{r}). \tag{20}$$

The vector potential reads:

$$V(\boldsymbol{r}) = g_{\omega}(\rho_v)\omega^0 + \tau_3 g_{\rho}(\rho_v)\rho^0 + e\frac{1+\tau_3}{2}A^0 + \Sigma_R^0, \tag{21}$$

and the rearrangement contribution is:

$$\Sigma_R^0 = g'_{\sigma}(\rho_v)\rho_s\sigma + g'_{\omega}(\rho_v)\rho_v\omega^0 + g'_{\rho}(\rho_v)\rho_{tv}\rho^0. \tag{22}$$

ρ_{tv} denotes the isovector density, i.e. the difference between the proton and the neutron vector density.

The `DIRQFAM` program package includes the very successful density-dependent meson-exchange relativistic energy functional DD-ME2 [6]. The induced single-particle Dirac Hamiltonian is obtained by calculating the functional derivative of the Dirac Hamiltonian with respect to the density:

$$\delta\hat{h} = \begin{bmatrix} \delta V + \delta S & -\boldsymbol{\sigma} \cdot \delta\boldsymbol{\Sigma} \\ -\boldsymbol{\sigma} \cdot \delta\boldsymbol{\Sigma} & \delta V - \delta S \end{bmatrix}. \tag{23}$$

$\delta S = \delta\Sigma_s$ denotes the induced scalar potential, while the $\delta V = \delta\Sigma^0 + \delta\Sigma_R^0$ and $\delta\boldsymbol{\Sigma}$ denote the time-like and space-like components of the induced vector potential, respectively. Below we present the detailed expressions for $\delta\Sigma_s$, $\delta\Sigma^0$, $\delta\Sigma_R^0$ and $\delta\boldsymbol{\Sigma}$. The value of function given in bracket $[\cdot]_{gs}$ denotes the ground state value of that function.

$$\delta\Sigma_s = [g_\sigma(\rho_v)]_{gs}\,\delta\sigma + \left[g'_\sigma(\rho_v)\sigma\right]_{gs}\delta\rho_v, \tag{24}$$

$$\delta\Sigma^0 = [g_\omega(\rho_v)]_{gs}\,\delta\omega^0 + \left[g'_\omega(\rho_v)\omega^0\right]_{gs}\delta\rho_v + \tau_3\left[g_\rho(\rho_v)\right]_{gs}\delta\rho^0 + \tau_3\left[g'_\rho(\rho_v)\rho^0\right]_{gs}\delta\rho_v + \frac{1+\tau_3}{2}\delta V_C, \tag{25}$$

$$\delta\Sigma^0_R = \left(\left[g''_\sigma(\rho_v)\rho_s\sigma\right]_{gs} + + \left[g''_\omega(\rho_v)\rho_v\omega^0\right]_{gs} + \left[g''_\rho(\rho_v)\rho_{tv}\rho^0\right]_{gs}\right)\delta\rho_v + \left[g'_\sigma(\rho_v)\sigma\right]_{gs}\delta\rho_s + \left[g'_\omega(\rho_v)\omega^0\right]_{gs}\delta\rho_v + \left[g'_\rho(\rho_v)\rho^0\right]_{gs}\delta\rho_{tv} + \left[g'_\sigma(\rho_v)\rho_s\right]_{gs}\delta\sigma + \left[g'_\omega(\rho_v)\rho_v\right]_{gs}\delta\omega^0 + \left[g'_\rho(\rho_v)\rho_{tv}\right]_{gs}\delta\rho^0, \tag{26}$$

$$\delta\boldsymbol{\Sigma} = [g_\omega(\rho_v)]_{gs}\,\delta\boldsymbol{\omega} + \tau_3\left[g_\rho(\rho_v)\right]_{gs}\delta\boldsymbol{\rho} + \frac{1+\tau_3}{2}\delta\boldsymbol{V}_C. \tag{27}$$

The induced meson fields are obtained by solving the Klein-Gordon equations:

$$\left[-\triangle + m_\sigma^2\right]\delta\sigma = -[g_\sigma(\rho_v)]_{gs}\,\delta\rho_s - \left[g'_\sigma(\rho_v)\rho_s\right]_{gs}\delta\rho_v, \tag{28}$$

$$\left[-\triangle + m_\omega^2\right]\delta\omega^0 = [g_\omega(\rho_v)]_{gs}\,\delta\rho_v + \left[g'_\omega(\rho_v)\rho_v\right]_{gs}\delta\rho_v, \tag{29}$$

$$\left[-\triangle + m_\rho^2\right]\delta\rho^0 = \left[g_\rho(\rho_v)\right]_{gs}\delta\rho_{tv} + \left[g'_\rho(\rho_v)\rho_{tv}\right]_{gs}\delta\rho_v, \tag{30}$$

$$\left[-\triangle + m_\omega^2\right]\delta\boldsymbol{\omega} = [g_\omega(\rho_v)]_{gs}\,\delta\boldsymbol{j}, \tag{31}$$

$$\left[-\triangle + m_\rho^2\right]\delta\boldsymbol{\rho} = \left[g_\rho(\rho_v)\right]_{gs}\delta\boldsymbol{j}_{tv}. \tag{32}$$

The time-like and space-like components of the induced Coulomb fields are calculated by solving the Poisson equation:

$$-\triangle\delta V_C = e^2\delta\rho_p \quad \text{and} \quad -\triangle\delta\boldsymbol{V}_C = e^2\delta\boldsymbol{j}_p, \tag{33}$$

where $\delta\rho_p$ and $\delta\boldsymbol{j}_p$ denote the induced proton density and current. The procedure of solving the Klein-Gordon and the Poisson equations in cylindrical coordinates is described in Appendix B and Appendix C.

2.2. Low-rank method for calculating induced densities and currents

In this section we explain the method used for calculating the induced densities and currents acting as the source terms for the induced potentials. In Appendix A we provide a detailed list of the expressions for induced densities and currents calculated in the simplex-y harmonic oscillator (HO) basis. Notice that (after symmetrization) all of them can be written as:

$$\delta S(z, r_\perp, \omega) = \sum_{\alpha_1,\alpha_2} A_{\alpha_1,\alpha_2}(\omega)\phi_{n_{z_1}}(z)\phi_{n_{z_2}}(z)\phi^{|\Lambda_1|}_{n_{r_1}}(r_\perp)\phi^{|\Lambda_2|}_{n_{r_2}}(r_\perp), \tag{34}$$

where $A_{\alpha_1,\alpha_2}(\omega)$ is block upper triangular matrix. Detailed definition of the index $\alpha = (d, n_z, n_r, \Lambda)$ can be found in Appendix A. Block structure of the $A_{\alpha_1,\alpha_2}(\omega)$ matrix depends on the excitation multipolarity K, e.g. for $K = 0$ one obtains block diagonal matrix. For higher values of the multipolarity K, the block structure of the $A_{\alpha_1,\alpha_2}(\omega)$ matrix is more complicated, but one can always deduce it thus making the multiplication with matrix $A_{\alpha_1,\alpha_2}(\omega)$ much less time consuming. In Fig. 1 we display an example of such block structure of matrix $A_{\alpha_1,\alpha_2}(\omega)$ calculated for the $K = 3$ multipolarity.

The source terms $\delta S(z^{i_{GH}}, r_\perp^{i_{GL}}, \omega)$ should be evaluated on the Gaussian quadrature grid points $\boldsymbol{r}^{i_G} = (z^{i_{GH}}, r_\perp^{i_{GL}})$. In principle, one could implement the sum in Eq. (34) directly by arranging the loops in some convenient order. However, it is more efficient to define the matrix:

$$\boldsymbol{\Phi}_{(\alpha,i_G)} = \phi_{n_z}(z^{i_{GH}})\phi^{|\Lambda|}_{n_r}(r_\perp^{i_{GL}}), \tag{35}$$

which is unchanged throughout QFAM iterations. Then the Eq. (34) can be written as:

$$\delta S(\boldsymbol{r}^{i_G}, \omega) = \mathrm{diag}\left[\boldsymbol{\Phi}^T A(\omega)\boldsymbol{\Phi}\right], \tag{36}$$

where diag[·] denotes the diagonal of a matrix. Since the HO basis functions $\phi_{n_z}(z)$ and $\phi^{|\Lambda|}_{n_r}(r_\perp)$ contain Hermite and Laguerre polynomials, which both satisfy recursive relations, rows of the matrix $\boldsymbol{\Phi}$ are linearly dependent. Consequently, the rank of the matrix $\boldsymbol{\Phi}$ is relatively low in comparison to its full rank.

For example, if HO simplex-y basis with $N_{\text{shells}} = 16$ is used, matrix $\boldsymbol{\Phi}$ has $1 \le \alpha \le 2109$ rows, while the rank of $\boldsymbol{\Phi}$ is only 171. Therefore, if $1 \le i^G \le 3200$ quadrature points are used, $\boldsymbol{\Phi}$ can be preprocessed via singular value decomposition and be written as a product:

$$\boldsymbol{\Phi} = \boldsymbol{U}_{\boldsymbol{\Phi}}\boldsymbol{V}_{\boldsymbol{\Phi}}, \tag{37}$$

where $\boldsymbol{U}_{\boldsymbol{\Phi}}$ is 2109×171 matrix, while $\boldsymbol{V}_{\boldsymbol{\Phi}}$ is 171×3200 matrix. Matrices $\boldsymbol{U}_{\boldsymbol{\Phi}}, \boldsymbol{V}_{\boldsymbol{\Phi}}$ are calculated and stored in the QFAM initialization phase, and are used during the QFAM iterations as a means to find the source terms on a Gaussian quadrature grid:

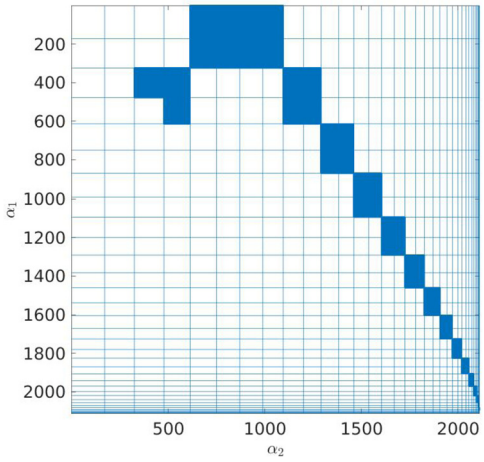

Fig. 1. (Color online) Example of the block structure of matrix $A_{\alpha_1,\alpha_2}(\omega)$ (see Eq. (34)) for $K = 3$ excitation multipolarity. Calculation was performed by using HO simplex-y basis with $N_{\text{shells}} = 16$ shells.

$$\delta S(\boldsymbol{r}^{i_G}, \omega) = \text{diag}\left[\boldsymbol{V}_{\boldsymbol{\Phi}}^T \left(\boldsymbol{U}_{\boldsymbol{\Phi}}^T A(\omega) \boldsymbol{U}_{\boldsymbol{\Phi}}\right) \boldsymbol{V}_{\boldsymbol{\Phi}}\right]. \tag{38}$$

$A(\omega)\boldsymbol{U}_{\boldsymbol{\Phi}}$ is a product of a block-matrix $A(\omega)$ and *tall-and-skinny* matrix $\boldsymbol{U}_{\boldsymbol{\Phi}}$, while $\boldsymbol{U}_{\boldsymbol{\Phi}}^T A(\omega)\boldsymbol{U}_{\boldsymbol{\Phi}}$ turns out to be a relatively small matrix, in our example 171×171 matrix. Then if we select the i_Gth column of a matrix $\boldsymbol{V}_{\boldsymbol{\Phi}}$, i.e. the vector $v_{i_G} = \boldsymbol{V}_{\boldsymbol{\Phi}}(:, i_G)$, the value $\delta S(\boldsymbol{r}^{i_G}, \omega)$ is calculated as a bilinear form with a small matrix $\boldsymbol{U}_{\boldsymbol{\Phi}}^T A(\omega)\boldsymbol{U}_{\boldsymbol{\Phi}}$ for each quadrature point as:

$$\delta S(\boldsymbol{r}^{i_G}, \omega) = v_{i_G}^T \left(\boldsymbol{U}_{\boldsymbol{\Phi}}^T A(\omega) \boldsymbol{U}_{\boldsymbol{\Phi}}\right) v_{i_G}. \tag{39}$$

However, in practice, due to more efficient use of cache, it is better to organize vectors v_{i_G} in batches of ~ 64 vectors (ideal number is machine dependent) and perform a batch-by-batch calculation instead. Otherwise the matrix $\boldsymbol{U}_{\boldsymbol{\Phi}}^T A(\omega)\boldsymbol{U}_{\boldsymbol{\Phi}}$ would likely have to go through the CPU cache for each vector v_{i_G} which reduces the performance.

Thus, utilizing the low-rank property of the matrix $\boldsymbol{\Phi}$, we have managed to write Eq. (34) in terms of basic linear algebra matrix operations. Taking advantage of a highly optimized BLAS Level 3 subroutines (which can run on any desired number of threads), the proposed method proved to be more efficient as compared to the straightforward loop implementation, even if the loop approach is adequately parallelized.

2.3. Generalized minimal residual method

In this section we describe the implementation of the generalized minimal residual method (GMRES) for the QFAM solver. We notice that although similar iterative methods have already been applied to various QRPA solvers [7–9], they are still not widely used.

2.3.1. Method description and convergence

The generalized minimal residual method is an iterative method for numerical solution of an indefinite non-Hermitian system of m linear equations $Ax = b$ with invertible A, where only mapping $x \mapsto Ax$ is required. It is assumed that the dimension m of matrix A is huge leading to massive memory requirements. In the nth iteration, GMRES approximates the solution x_n by a vector in a Krylov subspace with minimal residual norm. The Arnoldi iteration is used to find this vector x_n. More precisely, for the initial guess x_0 and initial residual $r_0 = b - Ax_0$, the nth Krylov subspace for this problem is:

$$K_n = \text{span}\left\{r_0, Ar_0, A^2 r_0, \ldots, A^{n-1} r_0\right\}. \tag{40}$$

The Arnoldi iteration is used to find orthonormal vectors $Q_n = [q_1, q_2, \ldots, q_n]$ which form a basis for K_n, where the first Arnoldi vector is $q_1 = r_0/\|r_0\|$. GMRES searches the vectors $x_n \in K_n$ in the Krylov spaces and thus it can be written as $x_n = x_0 + Q_n y_n$, for $y_n \in \mathbb{C}^n$, which is found by minimizing the residual norm (Euclidean norm is assumed $\|x\| = \sqrt{x^\dagger x}$):

$$\|r_n\| = \|b - Ax_n\| = \|b - Ax_0 - AQ_n y_n\| = \|r_0 - AQ_n y_n\|. \tag{41}$$

The Arnoldi process also produces an $(n+1) \times n$ upper Hessenberg matrix H_n such that $AQ_n = Q_{n+1} H_n$. Using that, Eq. (41) can be written as:

$$\|r_n\| = \|\|r_0\| q_1 - Q_{n+1} H_n y_n\| = \|Q_{n+1}(\|r_0\| e_1 - H_n y_n)\| = \|\|r_0\| e_1 - H_n y_n\|, \tag{42}$$

where we used that fact that the Euclidean norm is unitary invariant. Therefore, minimizing $\|r_n\|$ is a linear least squares problem with $(n+1) \times n$ matrix H_n and vector $\|r_0\| e_1 \in \mathbb{C}^{n+1}$. To summarize, GMRES method performs the following steps in the nth iteration:

1. Using H_{n-1} and Q_{n-1}, calculate H_n and $Q_n = [Q_{n-1}, q_n]$ with the Arnoldi iteration.
2. Find y_n which minimizes the residual norm $\|r_n\|$.

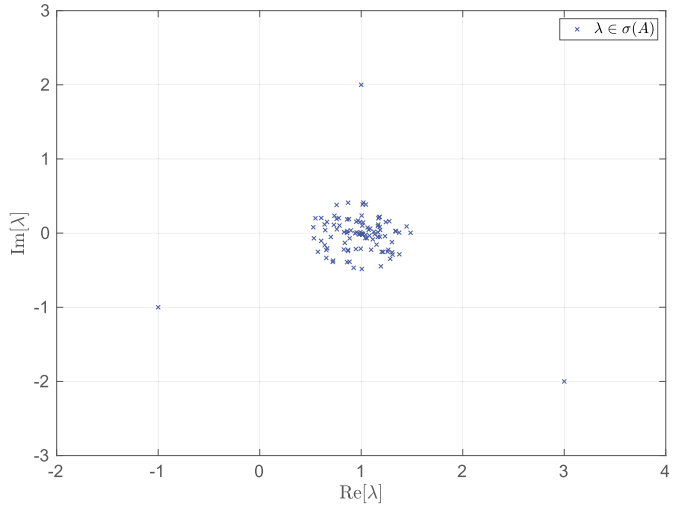

Fig. 2. (Color online) Spectrum $\sigma(A)$ of the matrix A with large cluster of eigenvalues contained within a circle $|\lambda - 1| \leq \frac{1}{2}$, and few eigenvalues located far away from the cluster.

3. If the relative residual error $\frac{\|b-Ax_n\|}{\|b\|} = \frac{\|r_n\|}{\|b\|}$ is below the desired tolerance, calculate $x_n = x_0 + Q_n y_n$. Otherwise, continue with the described process.

Notice that we need only the mapping $x \mapsto Ax$ in order to perform Arnoldi iterations. The GMRES method relies on the assumption that after a small number of iterations (small in comparison to the matrix dimension m), the vector x_n is already a good approximation of the solution x.

Suppose that matrix A can be diagonalized $A = V \operatorname{diag}[\lambda]_{\lambda\in\sigma(A)} V^{-1}$. Then one can prove the following relation [10]:

$$\frac{\|r_n\|}{\|r_0\|} \leq \kappa_2(V) \inf_{p\in\mathbb{P}_n} \max_{\lambda\in\sigma(A)} |p(\lambda)|, \tag{43}$$

where $\mathbb{P}_n$ is a set of polynomials of a maximal degree n with $p(0) = 1$, and $\kappa_2(V)$ is the condition number[1] of V. This suggests that if the eigenvectors matrix V is close to unitary matrix ($\kappa_2(V) \sim 1$), and the spectrum $\sigma(A)$ is localized, we can expect fast convergence of the GMRES method. More details on the GMRES method and its implementation can be found in Ref. [10].

2.3.2. Illustrative example

We will now show a typical case of matrix spectrum $\sigma(A)$, where one obtains fast convergence of the GMRES method. In Fig. 2 we plot the spectrum $\sigma(A)$ of the matrix A with large cluster of eigenvalues contained within a circle $|\lambda - 1| \leq \frac{1}{2}$, and few eigenvalues ($\lambda_1 = 3 - 2\mathrm{i},\ \lambda_2 = 1 + 2\mathrm{i},\ \lambda_3 = -1 - \mathrm{i}$) located far away from the cluster. For $n \geq 3$, let us consider the following polynomials:

$$p_n(\lambda) = (1-\lambda)^{n-3} \frac{(\lambda_1 - \lambda)(\lambda_2 - \lambda)(\lambda_3 - \lambda)}{\lambda_1\lambda_2\lambda_3}. \tag{44}$$

One can easily verify that $p_n \in \mathbb{P}_n$, i.e. $p_n(0) = 1$. Let us define a constant $C_{\lambda_1,\lambda_2,\lambda_3}$ as follows:

$$C_{\lambda_1,\lambda_2,\lambda_3} = \max_{|\lambda-1|\leq\frac{1}{2}} \left| \frac{(\lambda_1 - \lambda)(\lambda_2 - \lambda)(\lambda_3 - \lambda)}{\lambda_1\lambda_2\lambda_3} \right|. \tag{45}$$

Then the following relation holds:

$$\max_{\lambda\in\sigma(A)} |p_n(\lambda)| \leq \max_{|\lambda-1|\leq\frac{1}{2}} |p_n(\lambda)| \leq C_{\lambda_1,\lambda_2,\lambda_3} \max_{|\lambda-1|\leq\frac{1}{2}} |1-\lambda|^{n-3} \leq \frac{C_{\lambda_1,\lambda_2,\lambda_3}}{2^{n-3}}. \tag{46}$$

If the initial guess vector x_0 is simply set to a null vector $x_0 = 0$, then according to Eq. (43), the rate of decay of the relative residual error is at least exponentially fast:

$$\frac{\|r_n\|}{\|b\|} \sim \frac{1}{2^n}. \tag{47}$$

In practice, one usually obtains even faster convergence rate as compared to the rate that we have just estimated theoretically. One can repeat the same argument given here for a spectrum $\sigma(A)$ which is mostly contained a circle $|\lambda - 1| \leq \frac{1}{2}$ but now for the case of a spectrum $\sigma(A)$ mostly contained within an ellipse centered at 1 which doesn't contain the origin. Again, one can show [10] that even then the convergence is exponential.

[1] Recall that the condition number $\kappa_2(A)$ of invertible matrix A is defined as $\kappa_2(A) = ||A||_2||A^{-1}||_2$, where $||\cdot||_2$ is the matrix operator norm defined as: $||A||_2 = \max_{||x||_2=1} ||Ax||_2$. Notice that unitary matrices have condition number equal to one.

2.3.3. Application of the GMRES method for solving the QFAM equations

In the DIRQFAM code [1] we solve the QFAM equations:

$$(E_\mu + E_\nu - \omega_\gamma)X_{\mu\nu}(\omega_\gamma) = -\left(F^{20}_{\mu\nu}(\omega_\gamma) + \delta H^{20}_{\mu\nu}(\omega_\gamma)\right), \tag{48}$$

$$(E_\mu + E_\nu + \omega_\gamma)Y_{\mu\nu}(\omega_\gamma) = -\left(F^{02}_{\mu\nu}(\omega_\gamma) + \delta H^{02}_{\mu\nu}(\omega_\gamma)\right), \tag{49}$$

for a given complex frequency $\omega_\gamma = \omega + \gamma\mathrm{i}$. $F^{20}_{\mu\nu}(\omega_\gamma)$ and $F^{02}_{\mu\nu}(\omega_\gamma)$ correspond to the external field, while $H^{20}_{\mu\nu}(\omega_\gamma)$ and $H^{02}_{\mu\nu}(\omega_\gamma)$ depend on the induced single-particle Hamiltonian $\delta h_{kl}(\omega_\gamma)$ and pairing fields $\delta\Delta^{(+)}_{kl}(\omega_\gamma)$, $\left(\delta\Delta^{(-)}_{kl}(\omega_\gamma)\right)^*$ which in turn depend on the induced densities, i.e., on the QFAM amplitudes $X_{\mu\nu}(\omega_\gamma)$ and $Y_{\mu\nu}(\omega_\gamma)$. We denote the induced single-particle Hamiltonian and the pairing field by the symbol $\boldsymbol{x}(\omega_\gamma)$, i.e.,

$$\boldsymbol{x}(\omega_\gamma) = \left\{\delta h_{kl}(\omega_\gamma), \delta\Delta^{(+)}_{kl}(\omega_\gamma), \left(\delta\Delta^{(-)}_{kl}(\omega_\gamma)\right)^*\right\}. \tag{50}$$

Furthermore, $\boldsymbol{x}_i(\omega_\gamma)$ denotes the value calculated in the ith QFAM iteration. The goal is to obtain the same self-consistent value $\boldsymbol{x}_i(\omega_\gamma) = \boldsymbol{x}_{i+1}(\omega_\gamma)$ in two consecutive iterations, up to the given error tolerance. In the DIRQFAM code [1] the self-consistency was achieved by employing the modified Broyden's method [11].

The input for the ith QFAM iteration are the values induced single-particle Hamiltonian and pairing field from the previous iteration and the following transformations are performed:

$$\boldsymbol{x}_i(\omega_\gamma) \xrightarrow{1.} \left\{\delta H^{20}_{\mu\nu}(\omega_\gamma), \delta H^{02}_{\mu\nu}(\omega_\gamma)\right\} \xrightarrow{2.} \left\{X_{\mu\nu}(\omega_\gamma), Y_{\mu\nu}(\omega_\gamma)\right\} \xrightarrow{3.}$$
$$\left\{\delta\rho_{kl}(\omega_\gamma), \delta\kappa^{(\pm)}_{kl}(\omega_\gamma)\right\} \xrightarrow{4.} \left\{\delta\rho(\boldsymbol{r},\omega_\gamma), \delta\boldsymbol{j}(\boldsymbol{r},\omega_\gamma), P^{(\pm)}_{N_z,N_r}(\omega_\gamma)\right\} \xrightarrow{5.} \boldsymbol{x}_{i+1}(\omega_\gamma). \tag{51}$$

Following the formulae in our previous work [1], notice that steps 1., 3., 4. and 5. are linear transformations. For example, step 1. is a linear transformation performed by multiplying with Bogoliubov unitary matrix $\mathcal{W}$, while the numerical integration in step 5. can also be written as a linear transformation. Only step 2. is affine transformation which is actually the QFAM equation:

$$X_{\mu\nu}(\omega_\gamma) = -\left(F^{20}_{\mu\nu}(\omega_\gamma) + \delta H^{20}_{\mu\nu}(\omega_\gamma)\right)/(E_\mu + E_\nu - \omega_\gamma), \tag{52}$$

$$Y_{\mu\nu}(\omega_\gamma) = -\left(F^{02}_{\mu\nu}(\omega_\gamma) + \delta H^{02}_{\mu\nu}(\omega_\gamma)\right)/(E_\mu + E_\nu + \omega_\gamma). \tag{53}$$

If we set the residual interaction to zero, i.e., $\delta H^{20}_{\mu\nu}(\omega_\gamma) = \delta H^{02}_{\mu\nu}(\omega_\gamma) = 0$, and perform steps 2., 3., 4., and 5., we obtain the free response value $\boldsymbol{x}_{\mathrm{free}}(\omega_\gamma)$. Hence, the QFAM iteration (51) can be written as:

$$\boldsymbol{x}_{i+1}(\omega_\gamma) = \mathbb{T}(\omega_\gamma)\boldsymbol{x}_i(\omega_\gamma) + \boldsymbol{x}_{\mathrm{free}}(\omega_\gamma), \tag{54}$$

where $\mathbb{T}(\omega_\gamma)$ is a matrix describing the linear transformation induced by residual interaction which is ignored in free response. Size of the vector $\boldsymbol{x}(\omega_\gamma)$, and consequently the order of matrix $\mathbb{T}(\omega_\gamma)$, tends to be extremely large as the dimension of the configuration space increases. E.g. with only $N_{\mathrm{shells}} = 10$ oscillator shells used in the expansion of the Dirac spinors, the size of the vector $\boldsymbol{x}(\omega_\gamma)$ is $\approx 10^5$, while for $N_{\mathrm{shells}} = 20$ oscillator shells the size is $\approx 2\times 10^6$. Despite its size, the vector $\boldsymbol{x}_{\mathrm{free}}(\omega_\gamma)$ is easy to calculate, while the calculation of the matrix $\mathbb{T}(\omega_\gamma)$ can be prohibitively time consuming. However, the QFAM iteration (54) can be recognized as a means of calculating the mapping $\boldsymbol{x} \mapsto \left(\mathbb{I} - \mathbb{T}(\omega_\gamma)\right)\boldsymbol{x}$, for finding the self-consistent solution:

$$\left(\mathbb{I} - \mathbb{T}(\omega_\gamma)\right)\boldsymbol{x}(\omega_\gamma) = \boldsymbol{x}_{\mathrm{free}}(\omega_\gamma). \tag{55}$$

It turns out that the spectrum of the residual interaction matrix $\mathbb{T}(\omega_\gamma)$ contains relatively small number of eigenvalues far from zero. This is because, for a given excitation operator, the residual interaction tends to excite only a mall subset of particle-hole pairs. Hence, the eigenvalues of the matrix $\mathbb{I} - \mathbb{T}(\omega_\gamma)$ are clustered around 1, with relatively small number of the eigenvalues is scattered around the complex plane away from 1.

As an illustration, we have calculated the matrix $\mathbb{T}(\omega_\gamma)$ explicitly for deformed isotope ^{100}Zr and $J = 1$, $K = 0$ isovector excitation operator. The ground state deformation is $\beta \approx 0.47$ and we have used the DD-ME2 effective interaction and separable pairing [12,13]. However, we use only $N_{\mathrm{shells}} = 6$ shells, otherwise it would be difficult to fit the matrix $\mathbb{T}(\omega_\gamma)$ into the computer memory. In Fig. 3 we show the spectrum $\sigma(\mathbb{I} - \mathbb{T}(\omega_\gamma))$ for excitation frequency $\omega_\gamma = 30 + 0.05\mathrm{i}$ MeV. As we have anticipated, only a small fraction of eigenvalues are scattered away from 1. Motivated by the illustrative example shown in the previous subsection, this situation is well suited for the GMRES method, and thus in the DIRQFAM code we have substituted the previously used modified Broyden's method with GMRES solver.

To demonstrate the superiority of the GMRES method in terms of convergence speed, we perform a calculation of the isovector $J = 3$, $K = 1$ response of ^{240}Pu with deformed ground state $\beta \approx 0.28$, where we use $N_{\mathrm{shells}} = 20$ oscillator shells and smearing width $\gamma = 0.05$ MeV. Again, DD-ME2 interaction and separable pairing are used. We sweep across frequencies in range from 0 MeV to 50 MeV with an increment of 0.02 MeV. The response function is shown in Fig. 4 and it looks rather involved with many significant peaks. We compare the number of QFAM iterations performed by the modified Broyden's method where 70 vectors are retained in Broyden's history with the GMRES method using a maximum of 70 Arnoldi vectors. The same self-consistency tolerance is used in both methods. Modified Broyden's method took a total of 364527 QFAM iterations, i.e. on the average 146 QFAM iterations per frequency, while GMRES took a total of 107596 QFAM iterations,[2] i.e. on the average 44 QFAM iterations per frequency. Thus, for this example, GMRES method required 3.4 times

[2] We have taken into the account additional two QFAM iterations needed in GMRES, one for finding b, and another for finding the final solution x_n. We use $x_0 = 0$ as initial guess and thus the initial Arnoldi vector is $q_1 = r_0/\|r_0\| = b/\|b\|$, i.e. q_1 is given by b.

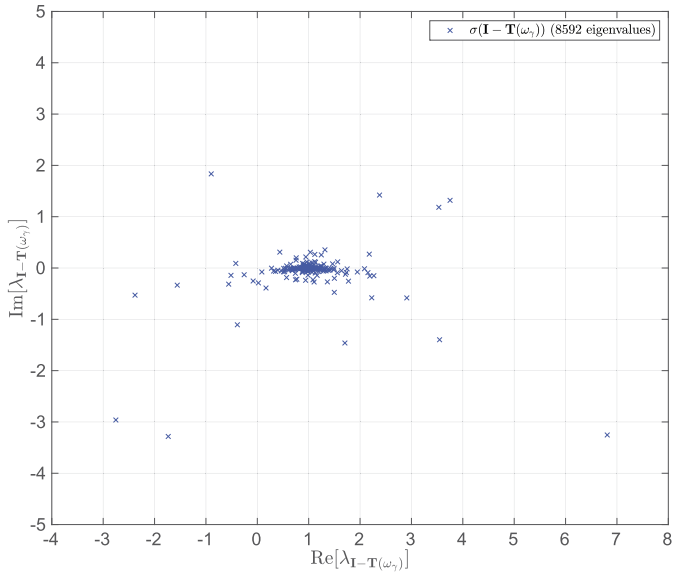

Fig. 3. (Color online) Example of spectrum of matrix $\sigma(\mathbb{I}-\mathbb{T}(\omega_\gamma))$ for isovector $J=1$, $K=0$ excitation of ^{100}Zr at $\omega_\gamma = 30+0.05\mathrm{i}$ MeV. We notice a large cluster of eigenvalues localized around 1, while only a small fraction of eigenvalues are scattered away from 1.

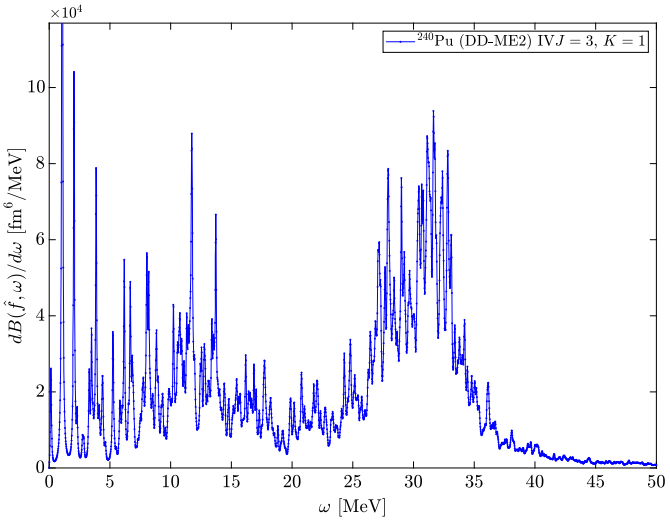

Fig. 4. (Color online) Isovector octupole $J=3$, $K=1$ response of ground state ^{240}Pu using DD-ME2 effective interaction and separable pairing. $\gamma = 0.05$ MeV is used as the complex part of the frequency ω_γ and $N_{\text{shells}} = 20(21)$ oscillator shells are used in the expansion of large (small) component of the spinor wave-function.

less QFAM iterations to find the response function compared to previously used Broyden's method. Maximum number of QFAM iterations for GMRES method was obtained at $\omega = 38.76$ MeV, where GMRES took 61 QFAM iterations, while Broyden's method took a maximum of 924 iterations at $\omega = 39.480$ MeV. In Fig. 5 we show the number of QFAM iterations for a given frequency for GMRES and Broyden's method. We can see that Broyden's method tends to have rather oscillating number of iterations while GMRES is approximately uniform regardless of the frequency ω.

For lighter nuclei with a simpler profile of the response function and for a larger smearing γ, (e.g. $\gamma \sim 0.5$ MeV) performance superiority of GMRES compared to Broyden's method is less pronounced. After experimenting with various nuclei and smearing width value γ, the GMRES method has always proved superior to the modified Broyden's method. Firstly, the number of QFAM iterations is reduced at least by a factor of two, which is a significant improvement. Secondly, the number of iterations performed with the GMRES method does not depend significantly on the excitation energy, contrary to the Broyden's method. Obviously, this is a great advantage when distributing the calculations on separate computing nodes.

2.3.4. Self-consistency tolerance and the number of Arnoldi vectors

Relative residual error $\frac{\|b-Ax_n\|}{\|b\|}$ of GMRES method applied on the QFAM problem is:

$$\frac{\|\boldsymbol{x}_{\text{free}}(\omega_\gamma) - (\mathbb{I}-\mathbb{T}(\omega_\gamma))\boldsymbol{x}_n(\omega_\gamma)\|}{\|\boldsymbol{x}_{\text{free}}(\omega_\gamma)\|} = \frac{\left\| \overbrace{\mathbb{T}(\omega_\gamma)\boldsymbol{x}_n(\omega_\gamma) + \boldsymbol{x}_{\text{free}}(\omega_\gamma)}^{\boldsymbol{x}_{n+1}(\omega_\gamma)} - \boldsymbol{x}_n(\omega_\gamma) \right\|}{\|\boldsymbol{x}_{\text{free}}(\omega_\gamma)\|}, \tag{56}$$

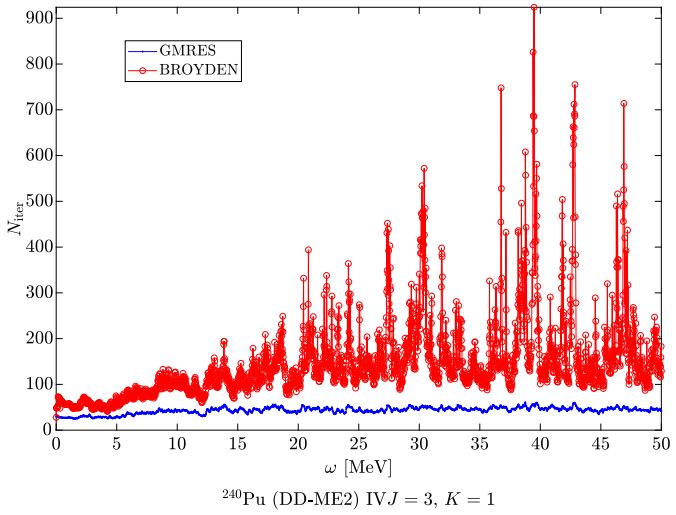

Fig. 5. (Color online) Number of iterations needed for both GMRES and Broyden's method at particular frequency for obtaining the response shown in Fig. 4.

which means that the GMRES method terminates when the norm of the difference between two vectors: $\boldsymbol{x}_{n+1}(\omega_\gamma)$ and $\boldsymbol{x}_n(\omega_\gamma)$ in two consecutive GMRES iterations (relative to the norm of the free response) is below a certain threshold tolerance ε:

$$\frac{\|\boldsymbol{x}_{n+1}(\omega_\gamma) - \boldsymbol{x}_n(\omega_\gamma)\|}{\|\boldsymbol{x}_{\text{free}}(\omega_\gamma)\|} < \varepsilon. \tag{57}$$

Previously in DIRQFAM code, we have used the stopping criterion:

$$\frac{\|\boldsymbol{x}_{i+1}(\omega_\gamma) - \boldsymbol{x}_i(\omega_\gamma)\|}{\|\boldsymbol{x}_i(\omega_\gamma)\|} < \varepsilon, \tag{58}$$

where $\boldsymbol{x}_i(\omega_\gamma)$ and $\boldsymbol{x}_{i+1}(\omega_\gamma)$ are two consecutive Broyden's vector. However, since it is more common in numerical mathematics to control the relative residual error $\frac{\|b-Ax_n\|}{\|b\|}$, rather than $\frac{\|b-Ax_n\|}{\|x_n\|}$, and because the self-consistent solution norm $\|\boldsymbol{x}(\omega_\gamma)\|$ is of the same order of magnitude as free response $\|\boldsymbol{x}_{\text{free}}(\omega_\gamma)\|$, we choose Eq. (57) as our stopping criterion in this version of the DIRQFAM code.

Experience has shown that for reasonable values of smearing $\gamma \approx 0.01 - 1$ MeV, if ε is set to $\varepsilon = 10^{-d}$, one obtains a strength function with at least $d - 1$ correct most significant digits. Thus we recommend using $\varepsilon = 10^{-6}$, however, we have included this parameter in a set of input parameters and the user can select the specific value depending on the desired accuracy. During an extensive testing, even in the most extreme cases, GMRES method converged with tolerance of $\varepsilon = 10^{-6}$ within approximately $50 - 60$ iterations, i.e. retaining $50 - 60$ Arnoldi vectors are enough, however we have also included the number of retained Arnoldi vectors in computer memory as an input parameter. We recommend using a value of 70 vectors. This means that if GMRES fails to satisfy the relative residual error tolerance ε within 70 iterations, the currently available GMRES solution after 70 iterations will be selected, and the corresponding strength function will be printed, where the final relative residual error will also be printed (with a message that the tolerance hasn't been satisfied). Thus, if the user insists on having a very small tolerance ε, which is not obtainable within 70 GMRES iterations, the user can easily increase the maximum allowed number of GMRES iterations via input parameter. Keep in mind that this increases the memory consumption of the program.

2.4. Nucleon localization function

For completeness, in this section we give a detailed derivation of the nucleon localization function introduced in Ref. [14,15] and describe the implementation in the new version of the DIRQFAM code. We start with a Hermitian density matrix $\hat{\rho} = \hat{\rho}^\dagger$ and define[3]:

$$\rho^q_{\sigma,\sigma'}(\boldsymbol{x}, \boldsymbol{x}') = \sum_{\alpha_1,\alpha_2} \hat{\rho}^q_{\alpha_1,\alpha_2}(\sigma, \sigma')\phi^*_{\alpha_2}(\boldsymbol{x}', \sigma')\phi_{\alpha_1}(\boldsymbol{x}, \sigma), \tag{59}$$

together with:

$$\rho^q_\sigma(\boldsymbol{x}) = \rho^q_{\sigma,\sigma}(\boldsymbol{x}, \boldsymbol{x}), \tag{60}$$

where σ denotes the spin index. Notice that, because $\hat{\rho}$ is hermitian, $\rho^q_\sigma(\boldsymbol{x})$ is real. The probability of finding two nucleons with the same spin σ and isospin q at spatial locations $\boldsymbol{x}$ and $\boldsymbol{x}'$ is given by:

$$P^q_\sigma(\boldsymbol{x}, \boldsymbol{x}') = \rho^q_\sigma(\boldsymbol{x})\rho^q_\sigma(\boldsymbol{x}') - \left|\rho^q_{\sigma,\sigma}(\boldsymbol{x}, \boldsymbol{x}')\right|^2. \tag{61}$$

On the other hand, the conditional probability of finding a nucleon with spin σ and isospin q at point $\boldsymbol{x}'$ when we know that another nucleon with the same spin and isospin is located at point $\boldsymbol{x}$ is given by the following expression:

[3] For more details about the density matrices we refer the reader to Appendix D of Ref. [16].

$$R^q_\sigma(\boldsymbol{x},\boldsymbol{x}') = \frac{P^q_\sigma(\boldsymbol{x},\boldsymbol{x}')}{\rho^q_\sigma(\boldsymbol{x})} = \rho^q_\sigma(\boldsymbol{x}') - \frac{\left|\rho^q_{\sigma,\sigma}(\boldsymbol{x},\boldsymbol{x}')\right|^2}{\rho^q_\sigma(\boldsymbol{x})}. \tag{62}$$

We fix the isospin value q and for simplicity omit the corresponding index in the following discussion. Because we are interested in the localization aspects, it is sufficient to consider only the local short-range behavior of the conditional probability, which one can obtain by performing a spherical averaging of $P_\sigma(\boldsymbol{x},\boldsymbol{x}')$ over a shell of radius δ about the point $\boldsymbol{x}$:

$$\left\langle P_\sigma(\boldsymbol{x},\boldsymbol{x}')\right\rangle_{\mathrm{AVG}(\boldsymbol{x},\delta)} = \frac{1}{4\pi\delta^2}\int\limits_{S(\boldsymbol{x},\delta)} P_\sigma(\boldsymbol{x},\boldsymbol{x}')dS_{\boldsymbol{x}'}. \tag{63}$$

We seek the limiting case $\delta \to 0^+$. First we consider a Taylor expansion over variable $\boldsymbol{x}'$ around $\boldsymbol{x}$:

$$\begin{aligned}\left|\rho_{\sigma,\sigma}(\boldsymbol{x},\boldsymbol{x}')\right|^2 &= \rho_\sigma(\boldsymbol{x})^2 + \sum_{i=1}^{3}\partial'_i\left|\rho_{\sigma,\sigma}(\boldsymbol{x},\boldsymbol{x}')\right|^2\Big|_{\boldsymbol{x}'=\boldsymbol{x}}(x'_i - x_i) + \\ &+ \frac{1}{2}\sum_{i,j=1}^{3}\partial'_i\partial'_j\left|\rho_{\sigma,\sigma}(\boldsymbol{x},\boldsymbol{x}')\right|^2\Big|_{\boldsymbol{x}'=\boldsymbol{x}}(x'_i - x_i)(x'_j - x_j) + \mathcal{O}(||\boldsymbol{x}' - \boldsymbol{x}||^3).\end{aligned} \tag{64}$$

One can trivially calculate the following spherical averages:

$$\left\langle (x'_i - x_i)\right\rangle_{\mathrm{AVG}(\boldsymbol{x},\delta)} = 0 \quad \text{and} \quad \left\langle (x'_i - x_i)(x'_j - x_j)\right\rangle_{\mathrm{AVG}(\boldsymbol{x},\delta)} = \delta_{i,j}\frac{\delta^2}{3}. \tag{65}$$

Using that, we obtain:

$$\left\langle\left|\rho_{\sigma,\sigma}(\boldsymbol{x},\boldsymbol{x}')\right|^2\right\rangle_{\mathrm{AVG}(\boldsymbol{x},\delta)} = \rho_\sigma(\boldsymbol{x})^2 + \frac{\delta^2}{6}\nabla^2_{\boldsymbol{x}'}\left|\rho_{\sigma,\sigma}(\boldsymbol{x},\boldsymbol{x}')\right|^2\Big|_{\boldsymbol{x}'=\boldsymbol{x}} + \mathcal{O}(\delta^3), \tag{66}$$

and similarly:

$$\left\langle\rho_\sigma(\boldsymbol{x}')\right\rangle_{\mathrm{AVG}(\boldsymbol{x},\delta)} = \rho_\sigma(\boldsymbol{x}) + \frac{\delta^2}{6}\nabla^2_{\boldsymbol{x}'}\rho_\sigma(\boldsymbol{x}')\Big|_{\boldsymbol{x}'=\boldsymbol{x}} + \mathcal{O}(\delta^3). \tag{67}$$

Using the Hermitian property of the density matrix $\hat{\rho}$ and formula $\nabla^2(fg) = g\nabla^2 f + f\nabla^2 g + 2\nabla f\cdot\nabla g$, it is straightforward to obtain:

$$\begin{aligned}\nabla^2_{\boldsymbol{x}'}\left|\rho_{\sigma,\sigma}(\boldsymbol{x},\boldsymbol{x}')\right|^2\Big|_{\boldsymbol{x}'=\boldsymbol{x}} &= \rho_\sigma(\boldsymbol{x})\left(\nabla^2\rho_\sigma(\boldsymbol{x}) - 2\sum_{\alpha_1,\alpha_2}\hat{\rho}_{\alpha_1,\alpha_2}(\sigma,\sigma)\nabla\phi^*_{\alpha_2}(\boldsymbol{x},\sigma)\cdot\nabla\phi_{\alpha_1}(\boldsymbol{x},\sigma)\right) \\ &+ 2\left|\sum_{\alpha_1,\alpha_2}\hat{\rho}_{\alpha_1,\alpha_2}(\sigma,\sigma)\phi_{\alpha_1}(\boldsymbol{x},\sigma)\nabla\phi^*_{\alpha_2}(\boldsymbol{x},\sigma)\right|^2,\end{aligned} \tag{68}$$

where the norm of a complex vector in the last term is $|v|^2 = |v_1|^2 + |v_2|^2 + |v_3|^2$. Inserting Eqs. (66), (67) and (68) into the spherical average of Eq. (61) and dividing by $\rho_\sigma(\boldsymbol{x})$, we obtain:

$$\left\langle R_\sigma(\boldsymbol{x},\boldsymbol{x}')\right\rangle_{\mathrm{AVG}(\boldsymbol{x},\delta)} = D_\sigma(\boldsymbol{x})\frac{\delta^2}{3} + \mathcal{O}(\delta^3), \tag{69}$$

where $D_\sigma(\boldsymbol{x})$ is defined as:

$$\begin{aligned}D_\sigma(\boldsymbol{x}) &= \sum_{\alpha_1,\alpha_2}\hat{\rho}_{\alpha_1,\alpha_2}(\sigma,\sigma)\nabla\phi^*_{\alpha_2}(\boldsymbol{x},\sigma)\cdot\nabla\phi_{\alpha_1}(\boldsymbol{x},\sigma) \\ &- \frac{1}{\rho_\sigma(\boldsymbol{x})}\left|\sum_{\alpha_1,\alpha_2}\hat{\rho}_{\alpha_1,\alpha_2}(\sigma,\sigma)\phi^*_{\alpha_2}(\boldsymbol{x},\sigma)\nabla\phi_{\alpha_1}(\boldsymbol{x},\sigma)\right|^2,\end{aligned} \tag{70}$$

and $\rho_\sigma(\boldsymbol{x})$ reads:

$$\rho_\sigma(\boldsymbol{x}) = \sum_{\alpha_1,\alpha_2}\hat{\rho}_{\alpha_1,\alpha_2}(\sigma,\sigma)\phi^*_{\alpha_2}(\boldsymbol{x},\sigma)\phi_{\alpha_1}(\boldsymbol{x},\sigma). \tag{71}$$

Notice that $D_\sigma(\boldsymbol{x})$ is real. In particular, if we insert $\hat{\rho}_{\alpha_1,\alpha_2}(\sigma,\sigma) = \delta_{\alpha_1,\alpha_2}$ into Eq. (70), we obtain the same result as given in Eq. (4) of Ref. [15]. Finally, we define the nucleon localization function as:

$$C_\sigma(\boldsymbol{x}) = \left[1 + \left(\frac{D_\sigma(\boldsymbol{x})}{\tau^\sigma_{\mathrm{TF}}(\boldsymbol{x})}\right)^2\right]^{-1}, \tag{72}$$

where the Thomas-Fermi kinetic energy density:

$$\tau_{\mathrm{TF}}^{\sigma}(\boldsymbol{x}) = \frac{3}{5}(6\pi)^{2/3}\rho_{\sigma}^{5/3}(\boldsymbol{x}), \tag{73}$$

acts as a natural scaling. The extreme case of ideal metallic bonding is realized for homogeneous matter where $\mathcal{C}_{\sigma}(\boldsymbol{x}) \sim 1/2$, a value that signals a region with a nearly homogeneous Fermi gas as is typical for metal electrons, nuclear matter, or neutron stars. The opposite regime is space regions where exactly one single-particle wave function contributes. Such a situation yields $D_{\sigma}(\boldsymbol{x}) \sim 0$, as it is not possible to find another spin-like state in the vicinity, and consequently $\mathcal{C}_{\sigma}(\boldsymbol{x}) \sim 1$, which signals localization.

In the DIRQFAM code [1] the induced density matrix is block diagonal and each block corresponds to the simplex-y quantum number $s = \pm i$:

$$\begin{aligned}\hat{\rho}(t) = &\begin{bmatrix} \underbrace{vv^{\dagger}}_{\rho_0} & 0 \\ 0 & (vv^{\dagger})^{T} \end{bmatrix} \\ &+ \eta e^{-\mathrm{i}\omega t}\begin{bmatrix} \delta\rho_1(\omega) & 0 \\ 0 & \delta\rho_2(\omega) \end{bmatrix} + \eta e^{+\mathrm{i}\omega t}\begin{bmatrix} \delta\rho_1^{\dagger}(\omega) & 0 \\ 0 & \delta\rho_2^{\dagger}(\omega) \end{bmatrix} + \mathcal{O}(\eta^2).\end{aligned} \tag{74}$$

Thus, up to the linear order in η, the density matrix $\hat{\rho}^{\dagger}(t) = \hat{\rho}(t)$ is indeed Hermitian.

In the DIRQFAM code, simplex-y is conserved quantum number with values $s = \pm\mathrm{i}$, and thus instead of the spin index σ in previous equations, we use the simplex-y index s. Since we are not interested in states with specific values of the simplex-y quantum number, we perform averaging over the simplex-y quantum number when inserting the simplex-y blocks from Eq. (74):

$$\begin{aligned}\hat{\rho}(s = +\mathrm{i}, s = +\mathrm{i}) &= \rho_0 + \eta e^{-\mathrm{i}\omega t}\delta\rho_1(\omega) + \eta e^{+\mathrm{i}\omega t}\delta\rho_1^{\dagger}(\omega) + \mathcal{O}(\eta^2), \\ \hat{\rho}(s = -\mathrm{i}, s = -\mathrm{i}) &= \rho_0^{T} + \eta e^{-\mathrm{i}\omega t}\delta\rho_2(\omega) + \eta e^{+\mathrm{i}\omega t}\delta\rho_2^{\dagger}(\omega) + \mathcal{O}(\eta^2),\end{aligned} \tag{75}$$

into the Eq. (70). Further details regarding the implementation of $\mathcal{C}(\boldsymbol{x})$ function are given in Appendix E. To summarize, the nucleon localization function (after the simplex averaging) can be written as:

$$\mathcal{C}(\boldsymbol{x}, t) = \mathcal{C}^0(z, r_{\perp}) + 2\eta\,\mathrm{Re}\left[e^{-\mathrm{i}\omega t}\delta\mathcal{C}(z, r_{\perp}, \omega)\right]\cos K\varphi + \mathcal{O}(\eta^2), \tag{76}$$

where $\mathcal{C}^0(\boldsymbol{x}) = \mathcal{C}^0(z, r_{\perp})$ is the ground state nucleon localization function.

2.5. Extraction of the QRPA transition matrix elements and eigenfrequencies

Although QFAM approach represents a very economical approach to the standard QRPA problem, it does not provide direct access to the QRPA eigenfrequencies Ω_i. However, in Ref. [17] a method based on the contour integration in the complex plane has been proposed that allows one to extract the QRPA transition matrix elements and eigenfrequencies from the QFAM calculation. In this section we provide only a brief overview and for detailed derivation we refer the reader to Ref. [17]. The starting point is the explicit connection between the QFAM strength function and the smeared QRPA strength function:

$$S(\hat{f}, \omega_{\gamma}) = -\sum_i \left(\frac{|\langle i|\hat{F}|0\rangle|^2}{\Omega_i - (\omega + \gamma\,\mathrm{i})} + \frac{|\langle 0|\hat{F}|i\rangle|^2}{\Omega_i + (\omega + \gamma\,\mathrm{i})}\right). \tag{77}$$

Similar connection can be established for the response function:

$$\begin{aligned}\frac{dB(\hat{f}, \omega_{\gamma})}{d\omega} &= -\frac{1}{\pi}\,\mathrm{Im}\,S(\hat{f}, \omega_{\gamma}) \\ &= \frac{\gamma}{\pi}\sum_i \left(\frac{|\langle i|\hat{F}|0\rangle|^2}{(\omega - \Omega_i)^2 + \gamma^2} - \frac{|\langle 0|\hat{F}|i\rangle|^2}{(\omega + \Omega_i)^2 + \gamma^2}\right).\end{aligned} \tag{78}$$

The discrete QRPA transition strength can be calculated by employing the Cauchy integral formula:

$$|\langle i|\hat{F}|0\rangle|^2 = \frac{1}{2\pi\,\mathrm{i}}\oint_{C_i} S(\hat{f}, \omega_{\gamma})d\omega_{\gamma}, \tag{79}$$

where C_i is a closed positively-oriented simple loop in complex plane that only encloses the ith positive first-order QRPA pole Ω_i. On the other hand, if the contour C in its interior $\mathrm{Int}\,C$ has other poles, the following relation holds:

$$\sum_{\Omega_i \in \mathrm{Int}\,C} |\langle i|\hat{F}|0\rangle|^2 = \frac{1}{2\pi\,\mathrm{i}}\oint_{C} S(\hat{f}, \omega_{\gamma})d\omega_{\gamma}. \tag{80}$$

As a first step one should run the QFAM calculation for sufficiently small smearing γ, and obtain a response profile $\frac{dB(\hat{f}, \omega_{\gamma})}{d\omega}$ providing a fair estimate for the locations of the QRPA poles Ω_i with significant transition probabilities $|\langle i|\hat{F}|0\rangle|^2$. After that, a contour integration of the strength function (80) with carefully selected contour C_i can be used to obtain the desired transition matrix elements. In principle, we can select any closed simple loop C_i, but for practical reasons we use a circle:

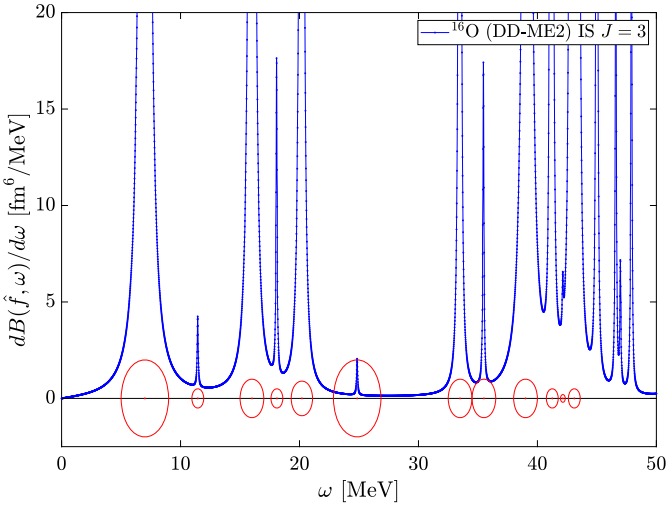

Fig. 6. (Color online) Isoscalar octupole response of ^{16}O, using DD-ME2 parameterization and $N_{\text{shells}} = 6$ oscillator shells for spinor expansion. Smearing $\gamma = 0.05$ MeV is used. Approximate positions of dominant eigenfrequencies Ω_i are evident. Circles schematically illustrate possible contours for integration.

Table 1
Comparison of transition matrix elements $|\langle i|\hat{F}|0\rangle|^2$ [fm^6] corresponding to Fig. 6 calculated by direct QRPA approach (second column) and QFAM contour integration method (third and fourth column). In third(fourth) column 20(50) quadrature points are used. First column contains the QRPA eigenfrequencies Ω_i [MeV].

Ω_i	QRPA $\lvert\langle i\rvert\hat{F}\lvert 0\rangle\rvert^2$	QFAM $\lvert\langle i\rvert\hat{F}\lvert 0\rangle\rvert^2$	QFAM $\lvert\langle i\rvert\hat{F}\lvert 0\rangle\rvert^2$
6.99207	3792.643	3786.191892	3786.190079
11.44044	4.025732	4.027805908	4.027805187
16.00261	1411.010	1410.827509	1410.823246
18.07308	18.13698	18.16427984	18.16384591
20.17490	695.1176	695.7697558	695.7685455
24.84325	2.073040	2.124316957	2.076412219
33.47279	290.0444	290.0960090	290.0886744
35.46012	18.41065	18.51968657	18.43513546
39.13158	2410.897	2410.598750	2410.565647
41.22860	253.4163	269.2637591	269.2620168
42.13009	2.739089	2.749169122	2.748494819

$$\omega_\gamma(\varphi) = \omega_0 + \omega_R e^{i\varphi}, \tag{81}$$

centered at $\omega = \omega_0$ with radius ω_R. The center and radius of the contour can easily be estimated from the response function profile in order that the contour encircles the desired pole Ω_i. Integral in Eq. (80) is numerically evaluated using a simple Newton-Cotes second order formula (Simpson's rule) with a given number of quadrature points.

The presented method of extracting the QRPA transition matrix elements and eigenfrequencies can be validated by comparing the calculated value with the results obtained by using the QRPA code that explicitly constructs and diagonalizes the QRPA matrix. As an example, we select spherical ^{16}O isotope because the available QRPA code [18] works for nuclei with spherically symmetric ground state. For the excitation operator we use the isoscalar octupole operator $r^3Y_{3,0}$. The calculation is performed by using the DD-ME2 energy density functional and large (small) components of the Dirac spinors are expanded in $N_{\text{shells}} = 6(7)$ oscillator shells. In Fig. 6 we show the response function calculated by using $\gamma = 0.05$ MeV smearing parameter. Approximate positions of the QRPA eigrenfrequencies Ω_i are evident and red circles denote the choices for the integration contours.

In Table 1 we show the results of the contour integration. First two columns are the QRPA eigenfrequencies and transition probabilities obtained by explicitly diagonalizing the QRPA matrix. Third column contains the results of the QFAM contour integration with 20 quadrature points while in the fourth column we list the results of contour integration with 50 quadrature points. The GMRES solver tolerance is set very low $\varepsilon = 10^{-9}$ in order to unambiguously check the convergence with respect to the number of quadrature points along the contour. We notice an excellent agreement between the direct QRPA approach and the QFAM calculation, especially since these calculations are entirely different. Furthermore, third and fourth column demonstrate that 20 quadrature points are enough for sufficient precision, however we recommend repeating the calculation with a larger number of quadrature points for convergence check. Notice that QFAM transition probabilities have to be multiplied by the factor $2J+1$, because spherical systems have the same response for all $|K| \leq J$.

For illustration of the contour C containing several eigenfrequencies, we used a circle centered at 43.1 MeV with radius of 0.5 MeV. There are two eigenfrequencies contained in that circle, namely $\Omega_i = 42.82$ MeV and $\Omega_i = 43.38$ MeV with transition matrix elements $|\langle i|\hat{F}|0\rangle|^2 = 402.9829$ [fm^6] and $|\langle i|\hat{F}|0\rangle|^2 = 511.1528$ [fm^6] respectively. The QFAM contour integration method (with 50 quadrature points) gives $\frac{1}{2\pi i}\oint_C S(\hat{f},\omega_\gamma)d\omega_\gamma = 914.3587$ [fm^6] compared to $402.9829 + 511.1528 = 914.1357$ [fm^6], which is consistent with Eq. (80).

There are methods [17] which can be used to calculate the QRPA eigenfrequencies Ω_i via contour integration. However, in practice, once we have the transition matrix element $|\langle i|\hat{F}|0\rangle|^2$, the corresponding eigenfrequency Ω_i can be well estimated by fitting the Lorentz curve to the corresponding part of the response function since in the vicinity of the Ω_i pole we have:

$$\frac{dB(\hat{f},\omega_\gamma)}{d\omega} \approx |\langle i|\hat{F}|0\rangle|^2 \frac{\gamma/\pi}{(\omega-\Omega_i)^2+\gamma^2}. \tag{82}$$

We have validated this approach in practice.

2.6. H^{11} part of the Hamiltonian

In Ref. [19] we have applied DIRQFAM code to provide an input for the quasiparticle vibration coupling (QVC) calculation. To facilitate systematic applications of the QFAM in similar calculations, we have included option for generating the necessary data.

We notice that the QVC calculation necessitates also the H^{11} part of the induced Hamiltonian and not just the H^{20} and H^{02} parts. Let us recall that the induced Hamiltonian in quasiparticle basis is:

$$\begin{bmatrix} \delta H^{11}(\omega) & \delta H^{20}(\omega) \\ -\delta H^{02}(\omega) & -\left(\delta H^{11}(\omega)\right)^T \end{bmatrix} = \begin{bmatrix} U & V^* \\ V & U^* \end{bmatrix}^\dagger \begin{bmatrix} \delta h(\omega) & \delta\Delta^{(+)}(\omega) \\ -\left(\delta\Delta^{(-)}(\omega)\right)^* & -\delta h^T(\omega) \end{bmatrix} \begin{bmatrix} U & V^* \\ V & U^* \end{bmatrix}. \tag{83}$$

Detailed formulae for $\delta H^{20}(\omega)$ and $\delta H^{02}(\omega)$ in the simplex-y HO basis are given in Ref. [1]. $\delta H^{11}(\omega)$ is given by:

$$\delta H^{11}(\omega) = U^\dagger \delta h(\omega) U - V^\dagger \delta h^T(\omega) V + U^\dagger \delta\Delta^{(+)}(\omega) V - V^\dagger \left(\delta\Delta^{(-)}(\omega)\right)^* U. \tag{84}$$

Following our notation from Ref. [1], $\delta H^{11}(\omega)$ in the simplex-y HO basis is given by:

$$\delta H^{11}(\omega) = \begin{bmatrix} \delta h_1^{11}(\omega) & 0 \\ 0 & \delta h_2^{11}(\omega) \end{bmatrix}, \tag{85}$$

where $\delta h_1^{11}(\omega)$ and $\delta h_2^{11}(\omega)$ are given by:

$$\delta h_1^{11}(\omega) = u^\dagger \delta h_1(\omega) u - v^\dagger \delta h_2^T(\omega) v + u^\dagger \delta\Delta_1^{(+)}(\omega) v + v^\dagger \left(\delta\Delta_1^{(-)}(\omega)\right)^\dagger u, \tag{86}$$

$$\delta h_2^{11}(\omega) = -\left(v^\dagger \delta h_1(\omega) v - u^\dagger \delta h_2^T(\omega) u - v^\dagger \delta\Delta_1^{(+)}(\omega) u - u^\dagger \left(\delta\Delta_1^{(-)}(\omega)\right)^\dagger v\right)^T. \tag{87}$$

Even though $\delta H^{11}(\omega)$ doesn't contribute to QFAM, we calculate and print them when the self-consistency is reached because $\delta H^{11}(\omega)$ (together with $\delta H^{20}(\omega)$ and $\delta H^{02}(\omega)$ which are needed in QFAM) evaluated at dominant eigenfrequencies $\omega = \Omega_i$ are used for extraction of the QVC vertex functions [19].

3. Description of the DIRQFAM v2.0.0 code

3.1. Structure of the DIRQFAM v2.0.0 code

In the previous version of the DIRQFAM code, all arrays were allocated statically via `common` blocks. The `dirqfam.par` file contained the information about the dimensions of the arrays, depending on the multipolarity K, the number of oscillator shells used for the expansion of the nucleon spinors and the number of the Gaussian quadrature mesh points in the $r_\perp$ and $z > 0$ direction. The `dirqfam.par` file had to be generated prior to the compilation process based on the data from the input file `dirqfam.dat`. Hence, each time the user wanted to change the input parameters relevant for the dimensions of the arrays, the entire code had to be recompiled. This legacy FORTRAN 77 concept is abandoned in the DIRQFAM v2.0.0 version of the code, where all arrays are dynamically allocated and stored in the Fortran `modules` which replaced `common` blocks and the compilation of the code is now performed in one step.

Similar to the previous version of the code, the main program calls various subroutines that read the data and perform the computation. The execution essentially consists of three parts. The first part uses the file `dirqfam.dat` to start the program, initializes and generates all the relevant information and allocate the arrays. The second part of the code carries out the self-consistent ground-state computation (for details please see Ref. [20]). The third part of the code performs the computation of the multipole response built upon the ground state. Most of the subroutines related to this part of the code are specified in details in Ref. [1] and here we describe the subroutines and functions added in the new version of the code.

- subroutine `init_mesons`: Allocates the memory for the relevant arrays and calculates $\mathcal{P}^{\Lambda_i}$ and $\mathcal{H}^{\Lambda_i}$ matrices defined in Appendix B.
- subroutine `fam_dmesons`: Solves the Klein-Gordon equation as described in Appendix B.
- function `fam_gmres`: Performs the GMRES step.
- subroutine `calculate_nuclocfunc`: Calculates the nucleon localization function as described in Appendix E.

Furthermore, several subroutines have undergone significant modifications in the new version of the code:

- subroutines `init_coulomb` and `fam_dcoulomb`: Space-like components of the Coulomb field are now also included;
- subroutine `fam_ddensdcurr`: The algorithm to calculate the Laplacians of densities and currents is modified as explained in Appendix A;

Table 2
Memory consumption of the program and the execution time per QFAM iteration for a given number of shells in HO basis. For comparison, values given in the parentheses are obtained with the old version of the code.

N_{shells}	Memory [GB]	Time [s]
10	0.42 (0.75)	0.24 (0.36)
12	0.68 (1.46)	0.49 (0.82)
14	1.11 (2.75)	0.99 (1.75)
16	1.77 (5.68)	1.82 (3.32)
18	2.83 (8.39)	3.23 (5.71)
20	4.40 (13.9)	5.52 (9.54)
22	6.65 (22.2)	8.97 (15.5)
24	11.1 (34.2)	14.1 (26.0)

- subroutine `fam_dpotentials`: The potentials related to the meson-exchange interactions are now included.

The rest of the subroutines and functions have undergone only minor modifications.

Furthermore, in comparison to the original version of the `DIRQFAM` code, we have significantly reduced the memory requirements. This is achieved by storing all block matrices entering the QFAM calculation as blocks of memory instead as full matrices dominantly populated by zero entries. We notice that this modification also improves the overall efficiency of the code due to better data caching.

We present the results of a benchmark calculation performed on Intel® Xeon® Platinum 8280 @ 2.70 GHz machine. BLAS and LAPACK are provided via Intel® oneAPI Math Kernel Library on a single thread. We select the isoscalar $J = 2$, $K = 2$ excitation with Gaussian quadrature grid: `NGH` $= 25$, `NGL` $= 50$. In order to compare the performance with the previous version of the code, the DD-PC1 parameterization of the Lagrangian is used and 70 Arnoldi vectors stored in the memory are used by the GMRES solver in this version of the code, while an analogous number of 70 Broyden's vectors are stored in the memory when the older version of the code is used. In Table 2 we give the memory consumption of the program and the execution time per QFAM iteration for a given number of shells N_{shells} in HO basis. Values in the parentheses are obtained with the old version of the code. We notice that the new version of the code requires roughly three times less memory for $N_{\text{shells}} \geq 16$.

3.2. Compilation and code execution

The programming language of the `DIRQFAM` v2.0.0 code is Fortan and the user should provide an implementation of the BLAS and LAPACK (version 3.1. or higher) linear algebra libraries. Since the code depends heavily on `zgemm`, `dgemm` and `dgemv` subroutines, the user should provide an efficient implementation of the BLAS library. We recommend an open source implementation OpenBLAS, or freely available Intel® oneAPI Math Kernel Library as a part of the Intel® oneAPI Base Toolkit.

The code is compiled by standard Makefile build automation which is set to work with the GFortran compiler. If the user invokes `make` command, the compilation of the code will produce the executable file `run`. The code is then executed by invoking the `./run` command. If the user invokes `make dbg`, the code is compiled in debug mode with various additional checks, and the executable `dbg` is generated. Since the executable produced in debug mode is considerably slower, this mode should be used only for testing and developing purposes. If OpenBLAS is employed, the command `export OPENBLAS_NUM_THREADS=4` can be invoked to select the number of threads used by OpenBLAS. If Intel® oneAPI Math Kernel Library is employed, the command `export MKL_NUM_THREADS=4` can be invoked to select the number of threads used by the Intel® oneAPI Math Kernel Library.

3.3. Input data

The input data are provided in the `dirqfam.dat` file, and are separated into two parts: i) input data related to the ground state calculation (detailed description can be found on pages 12 and 13 in Ref. [20]), ii) input data related to the QFAM calculation. The QFAM parameters interface include the following data.

- Calculation type (`calculation_type`) flag. Value `0`: Free response is calculated for a given range of energies. Value `1`: Self-consistent response is calculated for a given range of energies. Value `2`: Self-consistent response is calculated for a given energy and various data are printed. Value `3`: Self-consistent solution is calculated along a circular contour and the contour integral is calculated.
- Coulomb interaction flag (`include_coulomb`). If set to `0/1`, the Coulomb interaction is omitted/included in both the ground state and the QFAM calculation.
- Pairing interaction flag (`include_pairing`). If set to `0/1`, the pairing interaction is omitted/included in both the ground state and the QFAM calculation.
- Number of Gauss-Hermite (`NGH`) nodes in the $z > 0$ direction and number of Gauss-Laguerre (`NGL`) nodes in the $r_\perp$ direction. One should use at least:

$$\texttt{NGH} \geq \max\left\{N_{\text{shells}} + 1, N_{\text{shells}}^{(\text{mesons})}\right\}, \texttt{NGL} \geq \max\left\{2(N_{\text{shells}} + 1), N_{\text{shells}}^{(\text{mesons})}\right\}, \tag{88}$$

  where N_{shells} is the number of HO shells (`n0f`) used for Dirac spinor expansion and $N_{\text{shells}}^{(\text{mesons})}$ is the number of HO shells (`n0b`) used for the expansion of meson fields. We recommend fixing these values to `NGH=25` and `NGL=50`, since one rarely uses more than `n0f=24` and `n0b=50` shells.

- The smearing width γ (in MeV) used in the QFAM calculation (`gamma_smear`).
- Solver tolerance (`selfConsistencyTolerance`). Relative residual error tolerance ε for GMRES solver. We recommend using the value of `1.e-6`, which has shown to give the strength function accurate up to 5 most significant digits.
- Maximum number of Arnoldi vectors used in GMRES solver (`NoArnoldiVectors`). This is the limit on the number of QFAM solver steps. We recommend using the value of `70`. If the GMRES solver fails to satisfy the relative residual error tolerance, we recommend increasing this value, however keep in mind that this means larger memory consumption of the program.
- J (`J_multipole`) and K (`K_multipole`) multipolarity values that define[4] the multipole excitation operator $\hat{f}_{J,K}$. In the current implementation of the code their values are restricted to $0 \leq J \leq 5$, $0 \leq K \leq J$.
- The isospin (`Isospin`) value that determines whether the excitation is isoscalar (value `0`) or isovector (value `1`).
- Parameters that control the starting point (`omega_start`), the ending point (`omega_end`) and the increment (`delta_omega`) of the energy range over which the response is calculated. Relevant only if the calculation type flag is set to `0` or `1`.
- The energy (`omega_print`) for which the self-consistent solution is calculated if the calculation type is set to `2`.
- Parameters for the contour integration if the calculation type is set to `3`. The contour is a circle centered at `omega_center` (in MeV) with radius `omega_radius` (in MeV). Number of integration points used for contour integration is determined by the `NoContourPoints` parameter.

3.4. Output data

The output of the `DIRQFAM` v2.0.0 code is divided into two parts. Output file `dirhb.out`, located in the `output/GS_output` folder contains the information related to the ground state calculation (detailed description can be found in Ref. [20]). The output files relevant for the QFAM calculation are located in the `output/QFAM_output` folder. We notice that both folders `output/GS_output` and `output/QFAM_output` should be created by the user prior to running the code. The calculated strength function is written to the `strength.out` file.

If the calculation type flag is set to `2`, several additional output files are generated. Files `rhov_neut.out` and `rhov_prot.out` contain the ground state neutron/proton vector density and the induced neutron/proton vector density for the selected energy value `omega_print`. The values printed in these files, $\rho_v^0(z, r_\perp)$ and $\delta\rho_v(z, r_\perp, \omega)$, are suitable for visualization of the time dependent density:

$$\rho_v(\boldsymbol{r}, t) = \rho_v^0(z, r_\perp) + 2\eta \mathrm{Re}\left[e^{-\mathrm{i}\omega t}\delta\rho_v(z, r_\perp, \omega)\right]\cos K\varphi, \tag{89}$$

where superscript 0 denotes the ground state density. η denotes small real parameter quantifying deviation of the system from the ground state imposed by external perturbation (for precise definition see Eq. (8) in Ref. [1]). Files `jr_neut.out`, `jr_prot.out`, `jz_neut.out`, `jz_prot.out`, `jphi_neut.out` and `jphi_prot.out` contain the $r_\perp$, z and φ components of the induced neuron/proton current for the selected energy value `omega_print`. The values printed in these files, $\delta j_z(z, r_\perp, \omega)$, $\delta j_\perp(z, r_\perp, \omega)$, $\delta j_\varphi(z, r_\perp, \omega)$, are suitable for visualization of the time dependent currents:

$$j_z(\boldsymbol{r}, t) = 2\eta \mathrm{Re}\left[e^{-\mathrm{i}\omega t}\delta j_z(z, r_\perp, \omega)\right]\cos K\varphi, \tag{90}$$

$$j_\perp(\boldsymbol{r}, t) = 2\eta \mathrm{Re}\left[e^{-\mathrm{i}\omega t}\delta j_\perp(z, r_\perp, \omega)\right]\cos K\varphi, \tag{91}$$

$$j_\varphi(\boldsymbol{r}, t) = 2\eta \mathrm{Re}\left[e^{-\mathrm{i}\omega t}\delta j_\varphi(z, r_\perp, \omega)\right]\sin K\varphi. \tag{92}$$

Furthermore, nucleon localization functions for neutrons and protons are printed into files `nuclocfunc_neut.out` and `nuclocfunc_prot.out`. More precisely, the printed values $\mathcal{C}^0(z, r_\perp)$ and $\delta\mathcal{C}(z, r_\perp, \omega)$, allow one to reconstruct the time-dependent localization function as defined in Eq. (76). Finally, quantities useful for the QVC calculations are also printed out (see Sec. 2.6). Files `U_neut.out`, `U_prot.out`, `V_neut.out` and `V_prot.out` contain the ground state Bogoliubov U and V matrices in simplex-y HO basis for neutrons and protons, while files `qpenergy_neut.out` and `qpenergy_prot.out` contain the ground state quasiparticle energies E_μ for neutrons and protons. QFAM amplitudes $X(\omega)$ and $Y(\omega)$ are printed in files `X_neut.out`, `X_prot.out`, `Y_neut.out` and `Y_prot.out`. The matrix elements of the induced Hamiltonian in the quasiparticle basis $\delta H^{20}(\omega)$, $\delta H^{02}(\omega)$ and $\delta H^{11}(\omega)$ are printed in files `dH20_neut.out`, `dH20_prot.out`, `dH02_neut.out` and `dH02_prot.out`, `dH11_neut.out` and `dH11_prot.out`. Detailed description of the simplex-y HO basis is provided in the file `basis.out`.

If the calculation type flag is set to `3`, the file `strength.out` contains strength function and the result of the contour integration.

3.5. Test calculations

As a benchmark after the code has been compiled on a particular machine, we provide several test calculations along with the code. The `test1` folder contains the free response (`calculation_type=0`) calculation of the isoscalar $J = 2$, $K = 2$ response built on top of the prolate deformed ground state of the ^{152}Sm isotope. The `test2` folder contains three examples of the fully self-consistent (`calculation_type=1`) calculation: i) isoscalar $J = 2$, $K = 2$ response built on top of the prolate deformed ground state of the ^{152}Sm isotope, ii) isovector $J = 1$, $K = 0$ response built on top of the prolate deformed ground state of the ^{100}Zr isotope, iii) isoscalar $J = 3$, $K = 0$ response built on top of the oblate deformed ground state of the ^{28}Si isotope.

The `test3` folder contains the calculation for the isoscalar $J = 2$, $K = 0$ response built on top of the prolate deformed ground state of the ^{20}Ne isotope. The calculation is performed for fixed energy $\omega = 25$ MeV (`calculation_type=3`) with various additional output files produced. Since for heavier systems the output files become large, we have selected light ^{20}Ne isotope for this illustrative calculation.

[4] For detailed expressions for external operator we refer the reader to Eqs. (53) and (54) in Ref. [1].

An example of the contour integration calculation (`calculation_type=4`) is provided in the `test4` folder. Calculation is performed for isoscalar $J=3$, $K=0$ response built on top of the spherical ground state of the ^{16}O isotope. The selected circle contour is centered at $\omega_0 = 16$ MeV with radius of $\omega_R = 1$ MeV and 20 integration points.

Finally, folder `sphericalTest` contains an example of the fully self-consistent calculation of the isovector $J=5$, $0 \le K \le J$ response built on top of the spherical ^{16}O isotope. In this test we have numerically verified that the strength function for spherical nucleus does not depend on the quantum number K for a fixed value of the angular momentum J, owed to the Wigner-Eckart theorem.

Examples of input files for all test calculations are provided, together with the expected output files.

4. Summary

We have upgraded the `DIRQFAM` code [1] that was designed to calculate the multipole response of even-even axially symmetric deformed nuclei by employing the quasiparticle finite amplitude method built on top of the self-consistent mean-field models based on the relativistic nuclear energy density functional. In addition to several new features described in the manuscript, static memory allocation has been replaced by the dynamic memory allocation to facilitate the compiling of the code for users. The memory requirements are significantly reduced by reorganizing the way block matrices are stored in the memory of a computer. In conclusion, added new features and improvements should make systematic studies of collective modes in heavy deformed nuclei more accessible for most users.

Declaration of competing interest

The authors declare that they have no known competing financial interests or personal relationships that could have appeared to influence the work reported in this paper.

Data availability

I have shared my data/code at the Attache file step.

Acknowledgements

This work has been supported in part by the Croatian Science Foundation project Uncertainty quantification within the nuclear energy density framework (IP-2018-01-5987) and the QuantiXLie Centre of Excellence, a project cofinanced by the Croatian Government and European Union through the European Regional Development Fund - the Competitiveness and Cohesion Operational Programme (KK.01.1.1.01.0004).

Appendix A. Induced densities and currents

For completeness, in this section we provide detailed expressions for induced densities and currents. We recall the harmonic oscillator basis functions:

$$|n_z, n_r, \Lambda\rangle = \phi_{n_z}(z)\phi_{n_r}^{|\Lambda|}(r_\perp)\frac{e^{i\Lambda\varphi}}{\sqrt{2\pi}}, \tag{A.1}$$

where the complete definition is given in Appendix A of Ref. [1]. Set of indices $\alpha = (d, n_z, n_r, \Lambda)$ denotes an element of basis within a given simplex block, where $d = f$ denotes large, and $d = g$ small component of the Dirac spinor, respectively.

We recall [1] the selection rules for the induced density matrix in `DIRQFAM` code. For (α_1, α_2) such that $d_1 = d_2$, the matrix elements of $(\delta\rho_1(\omega) + \delta\rho_2(\omega))_{\alpha_1,\alpha_2}$ are zero if $|\Lambda_1 - \Lambda_2| \neq K$, while for $d_1 \neq d_2$ they are zero if $|\Lambda_1 + \Lambda_2 + 1| \neq K$. On the other hand, for (α_1, α_2) such that $d_1 \neq d_2$ the matrix elements of $(\delta\rho_1(\omega) - \delta\rho_2(\omega))_{\alpha_1,\alpha_2}$ are zero if $|\Lambda_1 - \Lambda_2| \neq K$. For simplicity, in the following discussion we omit the frequency ω in $\delta\rho_1(\omega), \delta\rho_2(\omega)$, and the cylindrical coordinates $z, r_\perp$ in the HO eigenfunctions $\phi_{n_z}(z)$ and $\phi_{n_r}^{|\Lambda|}(r_\perp)$. Below we list the expressions for the induced densities and currents:

$$\delta\rho_v(\mathbf{r},\omega) = \frac{\cos K\varphi}{2\pi} \sum_{\substack{\alpha_1,\alpha_2 \\ |\Lambda_1-\Lambda_2|=K}} (\delta\rho_1 + \delta\rho_2)_{\alpha_1,\alpha_2} A^{\rho_v}_{\alpha_1,\alpha_2} \phi_{n_{z_1}}\phi_{n_{z_2}}\phi^{|\Lambda_1|}_{n_{r_1}}\phi^{|\Lambda_2|}_{n_{r_2}}, \tag{A.2}$$

$$A^{\rho_v}_{\alpha_1,\alpha_2} = \begin{cases} +1 & \text{for} \quad d_1 = d_2, \\ 0 & \text{for} \quad d_1 \neq d_2, \end{cases} \tag{A.3}$$

$$\delta\rho_s(\mathbf{r},\omega) = \frac{\cos K\varphi}{2\pi} \sum_{\substack{\alpha_1,\alpha_2 \\ |\Lambda_1-\Lambda_2|=K}} (\delta\rho_1 + \delta\rho_2)_{\alpha_1,\alpha_2} A^{\rho_s}_{\alpha_1,\alpha_2} \phi_{n_{z_1}}\phi_{n_{z_2}}\phi^{|\Lambda_1|}_{n_{r_1}}\phi^{|\Lambda_2|}_{n_{r_2}}, \tag{A.4}$$

$$A^{\rho_s}_{\alpha_1,\alpha_2} = \begin{cases} +1 & \text{for} \quad d_1 = d_2 = f, \\ -1 & \text{for} \quad d_1 = d_2 = g, \\ 0 & \text{for} \quad d_1 \neq d_2, \end{cases} \tag{A.5}$$

$$\delta j_z(\mathbf{r},\omega) = \frac{\cos K\varphi}{2\pi} \sum_{\substack{\alpha_1,\alpha_2 \\ |\Lambda_1-\Lambda_2|=K}} (\delta\rho_1 - \delta\rho_2)_{\alpha_1,\alpha_2} A^{j_z}_{\alpha_1,\alpha_2} \phi_{n_{z_1}}\phi_{n_{z_2}}\phi^{|\Lambda_1|}_{n_{r_1}}\phi^{|\Lambda_2|}_{n_{r_2}}, \tag{A.6}$$

$$A^{j_z}_{\alpha_1,\alpha_2} = \begin{cases} 0 & \text{for} \quad d_1 = d_2, \\ +1 & \text{for} \quad d_1 \neq d_2 = f, \end{cases} \tag{A.7}$$

$$\delta j_\perp(\boldsymbol{r},\omega) = \frac{\cos K\varphi}{2\pi \mathrm{i}} \sum_{\substack{\alpha_1,\alpha_2 \\ |\Lambda_1+\Lambda_2+1|=K}} (\delta\rho_1+\delta\rho_2)_{\alpha_1,\alpha_2} A^{j_\perp}_{\alpha_1,\alpha_2} \phi_{n_{z_1}}\phi_{n_{z_2}}\phi^{|\Lambda_1|}_{n_{r_1}}\phi^{|\Lambda_2|}_{n_{r_2}}, \tag{A.8}$$

$$A^{j_\perp}_{\alpha_1,\alpha_2} = \begin{cases} 0 & \text{for} \quad d_1 = d_2, \\ +1 & \text{for} \quad d_1 = f \text{ and } d_2 = g, \\ -1 & \text{for} \quad d_1 = g \text{ and } d_2 = f, \end{cases} \tag{A.9}$$

$$\delta j_\varphi(\boldsymbol{r},\omega) = \frac{\sin K\varphi}{-2\pi \mathrm{i}} \sum_{\substack{\alpha_1,\alpha_2 \\ |\Lambda_1+\Lambda_2+1|=K}} (\delta\rho_1+\delta\rho_2)_{\alpha_1,\alpha_2} A^{j_\varphi}_{\alpha_1,\alpha_2} \phi_{n_{z_1}}\phi_{n_{z_2}}\phi^{|\Lambda_1|}_{n_{r_1}}\phi^{|\Lambda_2|}_{n_{r_2}}, \tag{A.10}$$

$$A^{j_\varphi}_{\alpha_1,\alpha_2} = \mathrm{sgn}(\Lambda_1+\Lambda_2+1) A^{j_\perp}_{\alpha_1,\alpha_2}. \tag{A.11}$$

In order to solve the Klein-Gordon equation for the space-like components of the currents, it is convenient to define: $\delta j_1 = (\delta j_\perp - \delta j_\varphi)/\sqrt{2}$ and $\delta j_2 = (\delta j_\perp + \delta j_\varphi)/\sqrt{2}$.[5] Explicit expressions for δj_1 and δj_2 are given below:

$$\delta j_1(z,r_\perp,\omega) = \frac{\sqrt{2}}{1+\delta_{K,0}} \frac{1}{2\pi \mathrm{i}} \sum_{\substack{\alpha_1,\alpha_2 \\ \Lambda_1+\Lambda_2+1=+K}} (\delta\rho_1+\delta\rho_2)_{\alpha_1,\alpha_2} A^{j_\perp}_{\alpha_1,\alpha_2} \phi_{n_{z_1}}\phi_{n_{z_2}}\phi^{|\Lambda_1|}_{n_{r_1}}\phi^{|\Lambda_2|}_{n_{r_2}}, \tag{A.12}$$

$$\delta j_2(z,r_\perp,\omega) = \frac{\sqrt{2}}{1+\delta_{K,0}} \frac{1}{2\pi \mathrm{i}} \sum_{\substack{\alpha_1,\alpha_2 \\ \Lambda_1+\Lambda_2+1=-K}} (\delta\rho_1+\delta\rho_2)_{\alpha_1,\alpha_2} A^{j_\perp}_{\alpha_1,\alpha_2} \phi_{n_{z_1}}\phi_{n_{z_2}}\phi^{|\Lambda_1|}_{n_{r_1}}\phi^{|\Lambda_2|}_{n_{r_2}}. \tag{A.13}$$

Next we show how to calculate the Laplacians of the induced densities and currents. Using Talmi-Moshinsky brackets, one can show that the induced densities $\delta\rho_v(z,r_\perp,\omega)$, $\delta\rho_s(z,r_\perp,\omega)$ and current $\delta j_z(z,r_\perp,\omega)$ can be written as linear combinations of the basis functions:

$$\left\{\phi_{N_z}(z,\tilde{b}_z)\phi^{|K|}_{N_r}(r_\perp,\tilde{b}_\perp)\right\},$$

with reduced oscillator length $\tilde{b}_0 = b_0/\sqrt{2}$. On the other hand, induced current $\delta j_1(z,r_\perp,\omega)$ is a linear combination of the basis functions:

$$\left\{\phi_{N_z}(z,\tilde{b}_z)\phi^{|K-1|}_{N_r}(r_\perp,\tilde{b}_\perp)\right\},$$

while the induced current $\delta j_2(z,r_\perp,\omega)$ is a linear combination of basis functions:

$$\left\{\phi_{N_z}(z,\tilde{b}_z)\phi^{|K+1|}_{N_r}(r_\perp,\tilde{b}_\perp)\right\}.$$

Finally, we can easily obtain expressions for the Laplacians of various densities and current components. For example, let us focus on $\delta\rho_v(z,r_\perp,\omega)$. As we have stated, $\delta\rho_v(z,r_\perp,\omega)$ can be written as:

$$\delta\rho_v(z,r_\perp,\omega) = \sum_{N_z,N_r} c_{N_z,N_r}\phi_{N_z}(z,\tilde{b}_z)\phi^{|K|}_{N_r}(r_\perp,\tilde{b}_\perp). \tag{A.14}$$

Essentially, we are interested in induced densities and currents evaluated only on a Gaussian quadrature grid points $(z^{i_{GH}}, r^{i_{GL}}_\perp)$ given by Gauss-Hermite and Gauss-Laguerre quadrature nodes. Once we have calculated the values of $\delta\rho_v(z^{i_{GH}}, r^{i_{GL}}_\perp,\omega)$, we can extract the coefficients c_{N_z,N_r} by numerical integration:

$$c_{N_z,N_r} = \int_{-\infty}^{+\infty} dz \int_0^{+\infty} r_\perp dr_\perp \delta\rho_v(z,r_\perp,\omega)\phi_{N_z}(z,\tilde{b}_z)\phi^{|K|}_{N_r}(r_\perp,\tilde{b}_\perp). \tag{A.15}$$

If we apply the Laplacian operator on the basis function, we obtain the following expression:

$$\begin{aligned}\triangle_{z,r_\perp,K}\phi_{N_z}(z,\tilde{b}_z)\phi^{|K|}_{N_r}(r_\perp,\tilde{b}_\perp) = &\left(\frac{z^2}{\tilde{b}_z^4} + \frac{r_\perp^2}{\tilde{b}_\perp^4} - \frac{2N_z+1}{\tilde{b}_z^2} - \frac{2(2N_r+K+1)}{\tilde{b}_\perp^2}\right)\times \\ &\times \phi_{N_z}(z,\tilde{b}_z)\phi^{|K|}_{N_r}(r_\perp,\tilde{b}_\perp),\end{aligned} \tag{A.16}$$

where the cylindrical Laplace operator for a given value of K is defined as:

$$\triangle_{z,r_\perp,K} = \frac{1}{r_\perp}\partial_{r_\perp}\left(r_\perp\partial_{r_\perp}\right) - \frac{K^2}{r_\perp^2} + \partial_z^2. \tag{A.17}$$

Now we can easily evaluate the Laplacian of the induced density $\delta\rho_v(z,r_\perp,\omega)$ on the Gaussian quadrature grid:

$$\triangle_{z,r_\perp,K}\delta\rho_v(z^{i_{GH}}, r^{i_{GL}}_\perp,\omega) = \sum_{N_zN_r} c_{N_z,N_r}\left(\triangle_{z,r_\perp,K}\phi_{N_z}(z^{i_{GH}},\tilde{b}_z)\phi^{|K|}_{N_r}(r^{i_{GL}}_\perp,\tilde{b}_\perp)\right), \tag{A.18}$$

using Eq. (A.16) and calculated coefficients c_{N_z,N_r} via Eq. (A.15).

[5] See Appendix B.

Appendix B. Klein-Gordon equation in cylindrical coordinates

The Klein-Gordon equation for the scalar field and the time-like components of the vector fields reads:

$$\left[-\triangle + m_\phi^2\right]\delta\Phi_0(\boldsymbol{r},\omega) = \delta S_0(\boldsymbol{r},\omega), \tag{B.1}$$

where $\delta\Phi_0(\boldsymbol{r},\omega)$ and $\delta S_0(\boldsymbol{r},\omega)$ denote the induced field and the source term, respectively (see Eqs. (28)-(30)). The angular dependence of each source terms originates from the angular dependence of the induced vector or scalar density[6] which corresponds to the $\cos K\varphi$ function [1], i.e.,

$$\delta S_0(\boldsymbol{r},\omega) = \delta S_0(z, r_\perp, \omega)\cos K\varphi. \tag{B.2}$$

One can show that the induced fields inherit the same angular dependence:

$$\delta\Phi_0(\boldsymbol{r},\omega) = \delta\Phi_0(z, r_\perp, \omega)\cos K\varphi. \tag{B.3}$$

The remaining part of the solution $\Phi_0(z, r_\perp, \omega)$ is calculated by solving the equation:

$$\left[-\triangle_{z,r_\perp,K} + m_\phi^2\right]\delta\Phi_0(z, r_\perp, \omega) = \delta S_0(z, r_\perp, \omega). \tag{B.4}$$

For the space-like components (see Eqs. (31)-(32)) of the vector fields, the Klein-Gordon equation reads:

$$\left[-\triangle + m_\phi^2\right]\delta\boldsymbol{\Phi}(\boldsymbol{r},\omega) = \delta\boldsymbol{S}(\boldsymbol{r},\omega). \tag{B.5}$$

The angular dependence of the space-like components of the source term includes both the $\cos K\varphi$ and the $\sin K\varphi$ functions [1]:

$$\begin{aligned}\delta\boldsymbol{S}(\boldsymbol{r},\omega) = {}& \delta S_z(z, r_\perp, \omega)\cos K\varphi\, \boldsymbol{e}_z + \delta S_\perp(z, r_\perp, \omega)\cos K\varphi\, \boldsymbol{e}_\perp \\ & + \delta S_\varphi(z, r_\perp, \omega)\sin K\varphi\, \boldsymbol{e}_\varphi.\end{aligned} \tag{B.6}$$

We express the $\boldsymbol{e}_\perp$ and $\boldsymbol{e}_\varphi$ unit vectors in terms of the Cartesian unit vectors $\boldsymbol{e}_x$ and $\boldsymbol{e}_y$:

$$\boldsymbol{e}_\perp = \cos\varphi\, \boldsymbol{e}_x + \sin\varphi\, \boldsymbol{e}_y, \quad \boldsymbol{e}_\varphi = -\sin\varphi\, \boldsymbol{e}_x + \cos\varphi\, \boldsymbol{e}_y, \tag{B.7}$$

thus obtaining:

$$\begin{aligned}\delta\boldsymbol{S}(\boldsymbol{r},\omega) = {}& \frac{1}{\sqrt{2}}\left[+\delta S_1(z, r_\perp, \omega)\cos(K-1)\varphi + \delta S_2(z, r_\perp, \omega)\cos(K+1)\varphi\right]\boldsymbol{e}_x \\ & + \frac{1}{\sqrt{2}}\left[-\delta S_1(z, r_\perp, \omega)\sin(K-1)\varphi + \delta S_2(z, r_\perp, \omega)\sin(K+1)\varphi\right]\boldsymbol{e}_y \\ & + \delta S_3(z, r_\perp, \omega)\cos K\varphi\boldsymbol{e}_z,\end{aligned} \tag{B.8}$$

where we have defined the following quantities:

$$\delta S_1(z, r_\perp, \omega) = \frac{1}{\sqrt{2}}\left[+\delta S_\perp(z, r_\perp, \omega) - \delta S_\varphi(z, r_\perp, \omega)\right], \tag{B.9}$$

$$\delta S_2(z, r_\perp, \omega) = \frac{1}{\sqrt{2}}\left[+\delta S_\perp(z, r_\perp, \omega) + \delta S_\varphi(z, r_\perp, \omega)\right], \tag{B.10}$$

$$\delta S_3(z, r_\perp, \omega) = S_z(z, r_\perp, \omega). \tag{B.11}$$

The angular dependence of the induced fields $\delta\boldsymbol{\Phi}(\boldsymbol{r},\omega)$ is inherited from the source terms $\delta\boldsymbol{S}(\boldsymbol{r},\omega)$:

$$\begin{aligned}\delta\boldsymbol{\Phi}(\boldsymbol{r},\omega) = {}& \delta\Phi_z(z, r_\perp, \omega)\cos K\varphi\, \boldsymbol{e}_z + \delta\Phi_\perp(z, r_\perp, \omega)\cos K\varphi\, \boldsymbol{e}_\perp \\ & + \delta\Phi_\varphi(z, r_\perp, \omega)\sin K\varphi\, \boldsymbol{e}_\varphi,\end{aligned} \tag{B.12}$$

and can be decomposed in an analogous way:

$$\begin{aligned}\delta\boldsymbol{\Phi}(\boldsymbol{r},\omega) = {}& \frac{1}{\sqrt{2}}\left[+\delta\Phi_1(z, r_\perp, \omega)\cos(K-1)\varphi + \delta\Phi_2(z, r_\perp, \omega)\cos(K+1)\varphi\right]\boldsymbol{e}_x \\ & + \frac{1}{\sqrt{2}}\left[-\delta\Phi_1(z, r_\perp, \omega)\sin(K-1)\varphi + \delta\Phi_2(z, r_\perp, \omega)\sin(K+1)\varphi\right]\boldsymbol{e}_y \\ & + \delta\Phi_3(z, r_\perp, \omega)\cos K\varphi\boldsymbol{e}_z.\end{aligned} \tag{B.13}$$

We insert Eqs. (B.13) and (B.8) in the Klein-Gordon equation (B.5), equate the terms with $\cos K\varphi$ and $\sin K\varphi$ angular dependence and obtain the equations for the components of the induced fields:

[6] Notice that the ground state densities are axially symmetric.

$$\left[-\triangle_{z,r_\perp,|K-1|}+m_\phi^2\right]\delta\Phi_1(z,r_\perp,\omega)=\delta S_1(z,r_\perp,\omega), \tag{B.14}$$

$$\left[-\triangle_{z,r_\perp,|K+1|}+m_\phi^2\right]\delta\Phi_2(z,r_\perp,\omega)=\delta S_2(z,r_\perp,\omega), \tag{B.15}$$

$$\left[-\triangle_{z,r_\perp,|K|}+m_\phi^2\right]\delta\Phi_3(z,r_\perp,\omega)=\delta S_3(z,r_\perp,\omega). \tag{B.16}$$

By employing the solutions of Eqs. (B.14)-(B.16), we can reconstruct the components of the meson fields in the cylindrical coordinate system:

$$\delta\Phi_\perp(z,r_\perp,\omega)=\frac{1}{\sqrt{2}}\left[+\delta\Phi_1(z,r_\perp,\omega)+\delta\Phi_2(z,r_\perp,\omega)\right], \tag{B.17}$$

$$\delta\Phi_\varphi(z,r_\perp,\omega)=\frac{1}{\sqrt{2}}\left[-\delta\Phi_1(z,r_\perp,\omega)+\delta\Phi_2(z,r_\perp,\omega)\right], \tag{B.18}$$

$$\delta\Phi_z(z,r_\perp,\omega)=\delta\Phi_3(z,r_\perp,\omega). \tag{B.19}$$

We expand the solutions of the Klein-Gordon equations (B.4), (B.14)-(B.16) in terms of the eigenfunctions of the axially symmetric harmonic oscillator potential. Detailed description of the HO basis can be found in Appendix A of Ref. [1], but here we use smaller oscillator length $\tilde{b}_0=b_0/\sqrt{2}$. This particular choice is a consequence of the fact that the induced densities and currents, i.e. the source terms of Klein-Gordon equations, are linear combinations of products of HO basis functions. Following the expressions for induced densities and currents given in Appendix A, the source terms can be written as:

$$\delta S_0(z,r_\perp,\omega)=\sum_{n_z,n_r}(\delta S_0)_{(n_z,n_r)}\phi_{n_z}(z,\tilde{b}_z)\phi_{n_r}^{|K|}(r_\perp,\tilde{b}_\perp), \tag{B.20}$$

$$\delta S_1(z,r_\perp,\omega)=\sum_{n_z,n_r}(\delta S_1)_{(n_z,n_r)}\phi_{n_z}(z,\tilde{b}_z)\phi_{n_r}^{|K-1|}(r_\perp,\tilde{b}_\perp), \tag{B.21}$$

$$\delta S_2(z,r_\perp,\omega)=\sum_{n_z,n_r}(\delta S_2)_{(n_z,n_r)}\phi_{n_z}(z,\tilde{b}_z)\phi_{n_r}^{|K+1|}(r_\perp,\tilde{b}_\perp), \tag{B.22}$$

$$\delta S_3(z,r_\perp,\omega)=\sum_{n_z,n_r}(\delta S_3)_{(n_z,n_r)}\phi_{n_z}(z,\tilde{b}_z)\phi_{n_r}^{|K|}(r_\perp,\tilde{b}_\perp). \tag{B.23}$$

Fields $\delta\Phi_i(z,r_\perp,\omega)$ are approximated by the same truncated expansion via coefficients $(\delta\Phi_i)_{(n_z,n_r)}$ for $i=0,1,2,3$.

Inserting each of the expansions (B.20)-(B.23) into their respective Klein-Gordon equations, we obtain a set of linear equations:

$$\sum_{n_z'n_r'}\mathcal{H}^{\Lambda_i}_{(n_z,n_r)(n_z',n_r')}(\delta\Phi_i)_{(n_z',n_r')}=(\delta S_i)_{(n_z,n_r)}, \tag{B.24}$$

with

$$\Lambda_i=\begin{cases}|K| & \text{for } i=0,3,\\ |K-1| & \text{for } i=1,\\ |K+1| & \text{for } i=2.\end{cases} \tag{B.25}$$

The $\mathcal{H}^K_{(n_z,n_r)(n_z',n_r')}$ matrix elements can be calculated analytically:

$$\begin{aligned}\mathcal{H}^K_{(n_z,n_r)(n_z',n_r')}=&\left[\frac{n_z+\frac{1}{2}}{\tilde{b}_z^2}+\frac{2n_r+K+1}{\tilde{b}_\perp^2}+m_\phi^2\right]\delta_{n_rn_r'}\delta_{n_zn_z'}\\ &-\frac{\delta_{n_rn_r'}}{2\tilde{b}_z^2}\left[\sqrt{(n_z+1)(n_z+2)}\delta_{n_z'n_z+2}+\sqrt{(n_z'+1)(n_z'+2)}\delta_{n_zn_z'+2}\right]\\ &+\frac{\delta_{n_zn_z'}}{\tilde{b}_\perp^2}\left[\sqrt{n_r(n_r+K)}\delta_{n_rn_r'+1}+\sqrt{n_r'(n_r'+K)}\delta_{n_r'n_r+1}\right],\end{aligned} \tag{B.26}$$

while the matrix elements of the source terms are calculated numerically by employing Gauss-Hermite and Gauss-Laguerre quadrature formulas:

$$(\delta S_i)_{(n_z,n_r)}=\int_{-\infty}^{+\infty}dz\int_0^{+\infty}r_\perp dr_\perp\phi_{n_z}(z,\tilde{b}_z)\phi_{n_r}^{|\Lambda_i|}(r_\perp,\tilde{b}_\perp)\delta S_i(z,r_\perp,\omega). \tag{B.27}$$

By inverting the set of equations (B.24), we obtain the coefficients $(\delta\Phi_i)_{(n_z,n_r)}$ that are used to calculate the induced fields $\delta\Phi_i(z,r_\perp,\omega)$ $(i=0,1,2,3)$.

In the DIRQFAM code, all fields $\delta S_i(z,r_\perp,\omega)$ in coordinate space are represented by their values on Gauss-Hermite and Gauss-Laguerre quadrature nodes $\delta S_i(z^{i_{GH}},r_\perp^{i_{GL}},\omega)$. By defining the matrix:

$$\mathbf{\Phi}^K_{(n_z,n_r)(i_{GH},i_{GL})}=\phi_{n_z}(z^{i_{GH}},\tilde{b}_z)\phi_{n_r}^{|K|}(r_\perp^{i_{GL}},\tilde{b}_\perp), \tag{B.28}$$

the numerical integration in Eq. (B.27) can be written as a matrix-vector multiplication:

$$(\delta S_i)_{(n_z,n_r)} = \sum_{i_{GH},i_{GL}} \mathbf{\Phi}^{\Lambda_i}_{(n_z,n_r)(i_{GH},i_{GL})} w_{b_z}^{i_{GH}} w_{b_\perp}^{i_{GL}} \delta S_i(z^{i_{GH}}, r_\perp^{i_{GL}}, \omega). \tag{B.29}$$

$w_{b_z}^{i_{GH}}$ and $w_{b_\perp}^{i_{GL}}$ denote the Gaussian quadrature weights. Inverting Eq. (B.24) yields:

$$\left[(\delta\Phi_i)_{(n_z,n_r)}\right]_{(n_z,n_r)} = \left(\mathcal{H}^{\Lambda_i}\right)^{-1} \mathbf{\Phi}^{\Lambda_i} \left[w_{b_z}^{i_{GH}} w_{b_\perp}^{i_{GL}} \delta S_i(z^{i_{GH}}, r_\perp^{i_{GL}}, \omega)\right]_{(i_{GH},i_{GL})}. \tag{B.30}$$

Because in practical calculations we need $\delta\Phi_i(z, r_\perp, \omega)$ evaluated on the Gaussian quadrature grid, the Eqs. (B.20)-(B.23) analogous for the induced meson fields $\delta\Phi_i(z, r_\perp, \omega)$ can be written as:

$$\begin{aligned}\left[\delta\Phi_i(z^{i_{GH}}, r_\perp^{i_{GL}}, \omega)\right]_{(i_{GH},i_{GL})} &= \left(\mathbf{\Phi}^{\Lambda_i}\right)^T \left(\mathcal{H}^{\Lambda_i}\right)^{-1} \mathbf{\Phi}^{\Lambda_i} \times \\ &\times \left[w_{b_z}^{i_{GH}} w_{b_\perp}^{i_{GL}} \delta S_i(z^{i_{GH}}, r_\perp^{i_{GL}}, \omega)\right]_{(i_{GH},i_{GL})}.\end{aligned} \tag{B.31}$$

$\mathcal{H}^K$ is a matrix representation of the linear operator $-\triangle_{z,r_\perp,K} + m_\phi^2$ in the truncated HO basis, and since $-\triangle_{z,r_\perp,K}$ is positive operator, the real matrix $\mathcal{H}^K$ is positive definite. Thus, we can find its Cholesky factorization $\mathcal{H}^K = \mathcal{L}^K \left(\mathcal{L}^K\right)^T$, for regular lower-triangular matrix $\mathcal{L}^K$. By defining the matrix $\mathcal{P}^K = \left(\mathcal{L}^K\right)^{-1} \mathbf{\Phi}^K$, we can write:

$$\begin{aligned}\left[\delta\Phi_i(z^{i_{GH}}, r_\perp^{i_{GL}}, \omega)\right]_{(i_{GH},i_{GL})} &= \left(\mathcal{P}^{\Lambda_i}\right)^T \mathcal{P}^{\Lambda_i} \times \\ &\times \left[w_{b_z}^{i_{GH}} w_{b_\perp}^{i_{GL}} \delta S_i(z^{i_{GH}}, r_\perp^{i_{GL}}, \omega)\right]_{(i_{GH},i_{GL})}.\end{aligned} \tag{B.32}$$

To summarize, if the source terms $\delta S_i(z, r_\perp, \omega)$ are given on the Gaussian quadrature grid, Eq. (B.32) provides a transformation for calculating the fields $\delta\Phi_i(z, r_\perp, \omega)$ on the same quadrature grid. We notice that the total computational cost consists of only two matrix-vector multiplications with a precomputed matrix $\mathcal{P}^{\Lambda_i}$.

Appendix C. Poisson equation in cylindrical coordinates

The procedure of solving the Poisson equation for the time-like component of the Coulomb field is described in details in Appendix D of Ref. [1] and in this section we focus on the space-like components, i.e. we solve the following equation:

$$-\triangle\delta\boldsymbol{V}_C(\boldsymbol{r}, \omega) = e^2 \delta\boldsymbol{j}_p(\boldsymbol{r}, \omega), \tag{C.1}$$

where $\delta\boldsymbol{j}_p(\boldsymbol{r}, \omega)$ denotes the induced proton current. The induced potential $\delta\boldsymbol{V}_C(\boldsymbol{r}, \omega)$ reads:

$$\delta\boldsymbol{V}_C(\boldsymbol{r}, \omega) = e^2 \int d\boldsymbol{r}' \frac{\delta\boldsymbol{j}_p(\boldsymbol{r}', \omega)}{|\boldsymbol{r} - \boldsymbol{r}'|}. \tag{C.2}$$

By using the identity:

$$\triangle_{\boldsymbol{r}'} |\boldsymbol{r} - \boldsymbol{r}'| = \frac{2}{|\boldsymbol{r} - \boldsymbol{r}'|}, \tag{C.3}$$

together with the integration by parts, the induced potential can be written in the following form [21]:

$$\delta\boldsymbol{V}_C(\boldsymbol{r}, \omega) = \frac{e^2}{2} \int d\boldsymbol{r}' |\boldsymbol{r} - \boldsymbol{r}'| \triangle_{\boldsymbol{r}'} \delta\boldsymbol{j}_p(\boldsymbol{r}', \omega). \tag{C.4}$$

The angular dependence of the induced currents includes both the $\cos K\varphi$ and $\sin K\varphi$ functions (see Appendix A):

$$\begin{aligned}\delta\boldsymbol{j}_p(\boldsymbol{r}, \omega) = &\delta j_{p,z}(z, r_\perp, \omega) \cos K\varphi\, \boldsymbol{e}_z + \delta j_{p,\perp}(z, r_\perp, \omega) \cos K\varphi\, \boldsymbol{e}_\perp \\ &+ \delta j_{p,\varphi}(z, r_\perp, \omega) \sin K\varphi\, \boldsymbol{e}_\varphi.\end{aligned} \tag{C.5}$$

We decompose the induced proton current into Cartesian components:

$$\begin{aligned}\delta\boldsymbol{j}_p(\boldsymbol{r}, \omega) = &\frac{1}{\sqrt{2}} \left[+\delta j_{p,1}(z, r_\perp, \omega) \cos(K-1)\varphi + \delta j_{p,2}(z, r_\perp, \omega) \cos(K+1)\varphi\right] \boldsymbol{e}_x \\ &+ \frac{1}{\sqrt{2}} \left[-\delta j_{p,1}(z, r_\perp, \omega) \sin(K-1)\varphi + \delta j_{p,2}(z, r_\perp, \omega) \sin(K+1)\varphi\right] \boldsymbol{e}_y \\ &+ \delta j_{p,3}(z, r_\perp, \omega) \cos K\varphi \boldsymbol{e}_z,\end{aligned} \tag{C.6}$$

where we have defined:

$$\delta j_{p,1}(z,r_\perp,\omega) = \frac{1}{\sqrt{2}}\left[\delta j_{p,\perp}(z,r_\perp,\omega) - \delta j_{p,\varphi}(z,r_\perp,\omega)\right], \tag{C.7}$$

$$\delta j_{p,2}(z,r_\perp,\omega) = \frac{1}{\sqrt{2}}\left[\delta j_{p,\perp}(z,r_\perp,\omega) + \delta j_{p,\varphi}(z,r_\perp,\omega)\right], \tag{C.8}$$

$$\delta j_{p,3}(z,r_\perp,\omega) = \delta j_{p,z}(z,r_\perp,\omega). \tag{C.9}$$

One can show that the induced Coulomb potential inherits the angular dependence from the induced proton current:

$$\begin{aligned}\delta \boldsymbol{V}_C(\boldsymbol{r},\omega) = {} & \delta V_{C,z}(z,r_\perp,\omega)\cos K\varphi\, \boldsymbol{e}_z + \delta V_{C,\perp}(z,r_\perp,\omega)\cos K\varphi\, \boldsymbol{e}_\perp \\ & + \delta V_{C,\varphi}(z,r_\perp,\omega)\sin K\varphi\, \boldsymbol{e}_\varphi,\end{aligned} \tag{C.10}$$

and can be decomposed in an analogous way:

$$\begin{aligned}\delta \boldsymbol{V}_C(\boldsymbol{r},\omega) = {} & \frac{1}{\sqrt{2}}\left[\delta V_{C,1}(z,r_\perp,\omega)\cos(K-1)\varphi + \delta V_{C,2}(z,r_\perp,\omega)\cos(K+1)\varphi\right]\boldsymbol{e}_x \\ & + \frac{1}{\sqrt{2}}\left[\delta V_{C,1}(z,r_\perp,\omega)\sin(K-1)\varphi - \delta V_{C,2}(z,r_\perp,\omega)\sin(K+1)\varphi\right]\boldsymbol{e}_y \\ & + \delta V_{C,3}(z,r_\perp,\omega)\cos K\varphi \boldsymbol{e}_z.\end{aligned} \tag{C.11}$$

Inserting Eqs. (C.6) and (C.11) into Eq. (C.4), and equating the terms with identical angular dependence leads to the following expressions:

$$\delta V_{C,1}(z,r_\perp,\omega) = \frac{e^2}{2}\int d\boldsymbol{r}'|\boldsymbol{r}-\boldsymbol{r}'|\triangle_{z',r'_\perp,|K-1|}\delta j_{p,1}(z',r'_\perp,\omega), \tag{C.12}$$

$$\delta V_{C,2}(z,r_\perp,\omega) = \frac{e^2}{2}\int d\boldsymbol{r}'|\boldsymbol{r}-\boldsymbol{r}'|\triangle_{z',r'_\perp,|K+1|}\delta j_{p,2}(z',r'_\perp,\omega), \tag{C.13}$$

$$\delta V_{C,3}(z,r_\perp,\omega) = \frac{e^2}{2}\int d\boldsymbol{r}'|\boldsymbol{r}-\boldsymbol{r}'|\triangle_{z',r'_\perp,|K|}\delta j_{p,3}(z',r'_\perp,\omega). \tag{C.14}$$

The detailed description of the procedure for solving integrals in Eqs. (C.12)-(C.14) by employing the Green's function can be found in Appendix D of Ref. [1]. Finally, the solutions of the integrals (C.12)-(C.14) are used to reconstruct the components of the induced Coulomb potential in the cylindrical coordinates:

$$\delta V_{C,\perp}(z,r_\perp,\omega) = \frac{1}{\sqrt{2}}\left[+\delta V_{C,1}(z,r_\perp,\omega) + \delta V_{C,2}(z,r_\perp,\omega)\right], \tag{C.15}$$

$$\delta V_{C,\varphi}(z,r_\perp,\omega) = \frac{1}{\sqrt{2}}\left[-\delta V_{C,1}(z,r_\perp,\omega) + \delta V_{C,2}(z,r_\perp,\omega)\right], \tag{C.16}$$

$$\delta V_{C,z}(z,r_\perp,\omega) = \delta V_{C,3}(z,r_\perp,\omega). \tag{C.17}$$

Appendix D. Induced single particle Hamiltonian

The induced single-particle Hamiltonian reads:

$$\delta\hat{h} = \begin{bmatrix}\delta V + \delta S & -\boldsymbol{\sigma}\cdot\delta\boldsymbol{\Sigma} \\ -\boldsymbol{\sigma}\cdot\delta\boldsymbol{\Sigma} & \delta V - \delta S\end{bmatrix}, \tag{D.1}$$

with:

$$\delta V(\boldsymbol{r},\omega) = \delta V(z,r_\perp,\omega)\cos K\varphi, \tag{D.2}$$

$$\delta S(\boldsymbol{r},\omega) = \delta S(z,r_\perp,\omega)\cos K\varphi, \tag{D.3}$$

$$\begin{aligned}\delta\boldsymbol{\Sigma}(\boldsymbol{r},\omega) = {} & \delta\Sigma_z(z,r_\perp,\omega)\cos K\varphi\, \boldsymbol{e}_z + \delta\Sigma_\perp(z,r_\perp,\omega)\cos K\varphi\, \boldsymbol{e}_\perp \\ & + \delta\Sigma_\varphi(z,r_\perp,\omega)\sin K\varphi\, \boldsymbol{e}_\varphi.\end{aligned} \tag{D.4}$$

One can show that the induced single-particle Hamiltonian is block diagonal in the simplex-y HO basis:

$$\delta h(\omega) = \begin{bmatrix}\delta h_1(\omega) & 0 \\ 0 & \delta h_2(\omega)\end{bmatrix}. \tag{D.5}$$

Next, we describe the calculation of the matrix elements of the $\delta h_1(\omega)_{\alpha_1,\alpha_2}$ block. We use the same notation $\alpha = (d, n_z, n_r, \Lambda)$ as in Appendix A. First introduce the auxiliary potentials:

$$\delta\Sigma_1(z,r_\perp,\omega) = \frac{1}{\sqrt{2}}\left[\delta\Sigma_\perp(z,r_\perp,\omega) - \delta\Sigma_\varphi(z,r_\perp,\omega)\right], \tag{D.6}$$

$$\delta\Sigma_2(z,r_\perp,\omega) = \frac{1}{\sqrt{2}}\left[\delta\Sigma_\perp(z,r_\perp,\omega) + \delta\Sigma_\varphi(z,r_\perp,\omega)\right], \tag{D.7}$$

$$\delta\Sigma_3(z,r_\perp,\omega) = \delta\Sigma_z(z,r_\perp,\omega). \tag{D.8}$$

For convenience, we omit the ω and $z, r_\perp$ variables in the following expressions.

If $d_1 = d_2 = f$ and $|\Lambda_1 - \Lambda_2| = K$, the matrix element $\delta h_1(\omega)_{\alpha_1,\alpha_2}$ reads:

$$\delta h_1(\omega)_{\alpha_1,\alpha_2} = \frac{1+\delta_{K,0}}{2} \int_{-\infty}^{+\infty} dz \int_0^{+\infty} r_\perp dr_\perp (\delta V + \delta S) \phi_{n_{z_1}} \phi_{n_{z_2}} \phi_{n_{r_1}}^{|\Lambda_1|} \phi_{n_{r_2}}^{|\Lambda_2|}. \tag{D.9}$$

If $d_1 = d_2 = g$ and $|\Lambda_1 - \Lambda_2| = K$, the matrix element $\delta h_1(\omega)_{\alpha_1,\alpha_2}$ reads:

$$\delta h_1(\omega)_{\alpha_1,\alpha_2} = \frac{1+\delta_{K,0}}{2} \int_{-\infty}^{+\infty} dz \int_0^{+\infty} r_\perp dr_\perp (\delta V - \delta S) \phi_{n_{z_1}} \phi_{n_{z_2}} \phi_{n_{r_1}}^{|\Lambda_1|} \phi_{n_{r_2}}^{|\Lambda_2|}. \tag{D.10}$$

If $d_1 \neq d_2$ and $\Lambda_1 + \Lambda_2 + 1 = +K$, the matrix element $\delta h_1(\omega)_{\alpha_1,\alpha_2}$ reads:

$$\delta h_1(\omega)_{\alpha_1,\alpha_2} = -\frac{1+\delta_{K,0}}{2} \sqrt{2} \mathrm{i} A^{\Sigma}_{\alpha_1,\alpha_2} \int_{-\infty}^{+\infty} dz \int_0^{+\infty} r_\perp dr_\perp \delta\Sigma_1 \phi_{n_{z_1}} \phi_{n_{z_2}} \phi_{n_{r_1}}^{|\Lambda_1|} \phi_{n_{r_2}}^{|\Lambda_2|}. \tag{D.11}$$

If $d_1 \neq d_2$ and $\Lambda_1 + \Lambda_2 + 1 = -K$, the matrix element $\delta h_1(\omega)_{\alpha_1,\alpha_2}$ reads:

$$\delta h_1(\omega)_{\alpha_1,\alpha_2} = -\frac{1+\delta_{K,0}}{2} \sqrt{2} \mathrm{i} A^{\Sigma}_{\alpha_1,\alpha_2} \int_{-\infty}^{+\infty} dz \int_0^{+\infty} r_\perp dr_\perp \delta\Sigma_2 \phi_{n_{z_1}} \phi_{n_{z_2}} \phi_{n_{r_1}}^{|\Lambda_1|} \phi_{n_{r_2}}^{|\Lambda_2|}. \tag{D.12}$$

If $d_1 \neq d_2$ and $|\Lambda_1 - \Lambda_2| = K$, the matrix element $\delta h_1(\omega)_{\alpha_1,\alpha_2}$ reads:

$$\delta h_1(\omega)_{\alpha_1,\alpha_2} = -\frac{1+\delta_{K,0}}{2} \int_{-\infty}^{+\infty} dz \int_0^{+\infty} r_\perp dr_\perp \delta\Sigma_3 \phi_{n_{z_1}} \phi_{n_{z_2}} \phi_{n_{r_1}}^{|\Lambda_1|} \phi_{n_{r_2}}^{|\Lambda_2|}. \tag{D.13}$$

The factor $A^{\Sigma}_{\alpha_1,\alpha_2}$ is equal to -1 if $d_1 = g$ and $d_2 = f$, otherwise it is equal to $+1$. All other matrix elements $\delta h_1(\omega)_{\alpha_1,\alpha_2}$ not listed above vanish. Notice that it is sufficient to calculate only the upper triangle of the matrix $\delta h_1(\omega)$, because there holds: $\delta h_1(\omega)_{\alpha_1,\alpha_2} = \delta h_1(\omega)_{\alpha_2,\alpha_1}$ for all (α_1, α_2), except for those pairs (α_1, α_2) satisfying $d_1 \neq d_2$ and $|\Lambda_1 + \Lambda_2 + 1| = K$, in which case there holds: $\delta h_1(\omega)_{\alpha_1,\alpha_2} = -\delta h_1(\omega)_{\alpha_2,\alpha_1}$.

The second block $\delta h_2(\omega)$ can be calculated directly from the first block $\delta h_1(\omega)$ because one can show that there holds: $\delta h_2(\omega)_{\alpha_1,\alpha_2} = \delta h_1(\omega)_{\alpha_1,\alpha_2}$ for all (α_1, α_2), except for those pairs (α_1, α_2) satisfying $d_1 \neq d_2$ and $|\Lambda_1 - \Lambda_2| = K$, in which case there holds: $\delta h_2(\omega)_{\alpha_1,\alpha_2} = -\delta h_1(\omega)_{\alpha_1,\alpha_2}$.

Integrals in Eqs. (D.9)-(D.13) are numerically calculated using the values of the induced potentials $\delta V(z^{i_{GH}}, r_\perp^{i_{GL}}, \omega)$, $\delta S(z^{i_{GH}}, r_\perp^{i_{GL}}, \omega)$ and $\delta\boldsymbol{\Sigma}(z^{i_{GH}}, r_\perp^{i_{GL}}, \omega)$ on the Gaussian quadrature grid. However, the domain of integration can be further reduced because functions $\phi_{n_z}(z)$ have a well defined parity: $\phi_{n_z}(-z) = (-1)^{n_z}\phi_{n_z}(z)$. For illustration, suppose we have a function $f(z, r_\perp)$ and want to calculate the integral:

$$I_{\alpha_1,\alpha_2} = \int_{-\infty}^{+\infty} dz \int_0^{+\infty} r_\perp dr_\perp f(z, r_\perp) \phi_{n_{z_1}} \phi_{n_{z_2}} \phi_{n_{r_1}}^{|\Lambda_1|} \phi_{n_{r_2}}^{|\Lambda_2|}. \tag{D.14}$$

Integral I_{α_1,α_2} can be written as:

$$I_{\alpha_1,\alpha_2} = \int_0^{+\infty} dz \int_0^{+\infty} r_\perp dr_\perp \left(f(z, r_\perp) + (-1)^{n_{z_1}+n_{z_2}} f(-z, r_\perp) \right) \phi_{n_{z_1}} \phi_{n_{z_2}} \phi_{n_{r_1}}^{|\Lambda_1|} \phi_{n_{r_2}}^{|\Lambda_2|}. \tag{D.15}$$

Thus, if we have the values $f(z^{i_{GH}}, r_\perp^{i_{GL}})$ on Gaussian quadrature grid, we can calculate:

$$f_0(z^{i_{GH}}, r_\perp^{i_{GL}}) = f(+z^{i_{GH}}, r_\perp^{i_{GL}}) + f(-z^{i_{GH}}, r_\perp^{i_{GL}}), \tag{D.16}$$

$$f_1(z^{i_{GH}}, r_\perp^{i_{GL}}) = f(+z^{i_{GH}}, r_\perp^{i_{GL}}) - f(-z^{i_{GH}}, r_\perp^{i_{GL}}), \tag{D.17}$$

only for $z^{i_{GH}} > 0$, and then depending on the parity of $n_{z_1} + n_{z_2}$ use f_0 or f_1 for calculating I_{α_1,α_2}, but now integrating only for $z^{i_{GH}} > 0$, thus reducing the number of operations by half.

Appendix E. Nucleon localization function

Here we derive the expression for the induced nucleon localization function given in Eq. (72). First we calculate the terms appearing in Eq. (70). Following the notation given in Appendix A of Ref. [1], first we calculate the following matrix elements:

$$
\begin{aligned}
&\langle n_{z1}, n_{r_1}, \Lambda_1; \pm\mathrm{i}|\overleftarrow{\nabla}\,\overrightarrow{\nabla}|n_{z_2}, n_{r_2}, \Lambda_2; \pm\mathrm{i}\rangle = \\
&+ \partial_z\phi_{n_{z_1}}(z)\partial_z\phi_{n_{z_2}}(z)\phi^{|\Lambda_1|}_{n_{r_1}}(r_\perp)\phi^{|\Lambda_2|}_{n_{r_2}}(r_\perp)\frac{\cos((\Lambda_1-\Lambda_2)\varphi)}{2\pi} \\
&+ \phi_{n_{z_1}}(z)\phi_{n_{z_2}}(z)\partial_{r_\perp}\phi^{|\Lambda_1|}_{n_{r_1}}(r_\perp)\partial_{r_\perp}\phi^{|\Lambda_2|}_{n_{r_2}}(r_\perp)\frac{\cos((\Lambda_1-\Lambda_2)\varphi)}{2\pi} \\
&+ \phi_{n_{z_1}}(z)\phi_{n_{z_2}}(z)\phi^{|\Lambda_1|}_{n_{r_1}}(r_\perp)\phi^{|\Lambda_2|}_{n_{r_2}}(r_\perp)\frac{\Lambda_1\Lambda_2}{r_\perp^2}\frac{\cos((\Lambda_1-\Lambda_2)\varphi)}{2\pi},
\end{aligned}
\tag{E.1}
$$

$$
\begin{aligned}
&\langle n_{z1}, n_{r_1}, \Lambda_1; \pm\mathrm{i}|\overrightarrow{\nabla}|n_{z_2}, n_{r_2}, \Lambda_2; \pm\mathrm{i}\rangle = \\
&+ \left(\phi_{n_{z_1}}(z)\partial_z\phi_{n_{z_2}}(z)\phi^{|\Lambda_1|}_{n_{r_1}}(r_\perp)\phi^{|\Lambda_2|}_{n_{r_2}}(r_\perp)\frac{\cos((\Lambda_1-\Lambda_2)\varphi)}{2\pi}\right)\boldsymbol{e}_z \\
&+ \left(\phi_{n_{z_1}}(z)\phi_{n_{z_2}}(z)\phi^{|\Lambda_1|}_{n_{r_1}}(r_\perp)\partial_{r_\perp}\phi^{|\Lambda_2|}_{n_{r_2}}(r_\perp)\frac{\cos((\Lambda_1-\Lambda_2)\varphi)}{2\pi}\right)\boldsymbol{e}_\perp \\
&+ \left(\phi_{n_{z_1}}(z)\phi_{n_{z_2}}(z)\phi^{|\Lambda_1|}_{n_{r_1}}(r_\perp)\phi^{|\Lambda_2|}_{n_{r_2}}(r_\perp)\frac{\Lambda_2}{r_\perp}\frac{\sin((\Lambda_1-\Lambda_2)\varphi)}{2\pi}\right)\boldsymbol{e}_\varphi.
\end{aligned}
\tag{E.2}
$$

Notice that the previous matrix elements are all real. We will drop the frequency ω and coordinate $(z, r_\perp, \varphi)$ variables for brevity and focus our attention on the second term in Eq. (70). Again we use the notation $\alpha = (d, n_z, n_r, \Lambda)$ for index of basis vector within the given simplex block. For each simplex $s = \pm\mathrm{i}$ block there holds:

$$
\begin{aligned}
&\mathrm{Re}\left[\sum_{\alpha_1,\alpha_2}\left(\rho_0^{\prime T} + \eta e^{-\mathrm{i}\omega t}\delta\rho_{1/2} + \eta e^{+\mathrm{i}\omega t}\delta\rho^\dagger_{1/2}\right)_{\alpha_1,\alpha_2}\langle\alpha_2; \pm i|\overrightarrow{\nabla}|\alpha_1; \pm i\rangle\right] = \\
&\sum_{\substack{\alpha_1,\alpha_2\\ d_1=d_2}}\mathrm{Re}\left[\rho_0^{\prime T}\right]_{\alpha_1,\alpha_2}\frac{\langle\alpha_2; \pm\mathrm{i}|\overrightarrow{\nabla}|\alpha_1; \pm\mathrm{i}\rangle + \langle\alpha_1; \pm\mathrm{i}|\overrightarrow{\nabla}|\alpha_2; \pm\mathrm{i}\rangle}{2} \\
&+ \sum_{\substack{\alpha_1,\alpha_2\\ d_1=d_2}} 2\eta\,\mathrm{Re}\left[e^{-\mathrm{i}\omega t}\delta\rho_{1/2}\right]_{\alpha_1,\alpha_2}\frac{\langle\alpha_2; \pm\mathrm{i}|\overrightarrow{\nabla}|\alpha_1; \pm\mathrm{i}\rangle + \langle\alpha_1; \pm\mathrm{i}|\overrightarrow{\nabla}|\alpha_2; \pm\mathrm{i}\rangle}{2}.
\end{aligned}
\tag{E.3}
$$

Since we are averaging over the simplex number $s = \pm\mathrm{i}$, instead of $\rho_0^{\prime T}$ and $\delta\rho_{1/2}$, we use $\frac{1}{2}\left(\rho_0 + \rho_0^T\right)$ and $\frac{1}{2}(\delta\rho_1 + \delta\rho_2)$. For (α_1, α_2) such that $d_1 = d_2$, matrix $(\rho_0)_{\alpha_1,\alpha_2}$ has selection rule $|\Lambda_1 - \Lambda_2| = 0$, while matrix $\frac{1}{2}(\delta\rho_1 + \delta\rho_2)_{\alpha_1,\alpha_2}$ has $|\Lambda_1 - \Lambda_2| = K$. Thus, if we define:

$$
f_z^0 = \sum_{\substack{\alpha_1,\alpha_2\\ d_1=d_2\\ |\Lambda_1-\Lambda_2|=0}}\mathrm{Re}[\rho_0]_{\alpha_1,\alpha_2}\frac{\partial_z\phi_{n_{z_1}}\phi_{n_{z_2}} + \phi_{n_{z_1}}\partial_z\phi_{n_{z_2}}}{2}\phi^{|\Lambda_1|}_{n_{r_1}}\phi^{|\Lambda_2|}_{n_{r_2}}\frac{1}{2\pi},
\tag{E.4}
$$

$$
f_\perp^0 = \sum_{\substack{\alpha_1,\alpha_2\\ d_1=d_2\\ |\Lambda_1-\Lambda_2|=0}}\mathrm{Re}[\rho_0]_{\alpha_1,\alpha_2}\phi_{n_{z_1}}\phi_{n_{z_2}}\frac{\partial_{r_\perp}\phi^{|\Lambda_1|}_{n_{r_1}}\phi^{|\Lambda_2|}_{n_{r_2}} + \phi^{|\Lambda_1|}_{n_{r_1}}\partial_{r_\perp}\phi^{|\Lambda_2|}_{n_{r_2}}}{2}\frac{1}{2\pi},
\tag{E.5}
$$

$$
\delta f_z = \sum_{\substack{\alpha_1,\alpha_2\\ d_1=d_2\\ |\Lambda_1-\Lambda_2|=K}}\left(\frac{\delta\rho_1+\delta\rho_2}{2}\right)_{\alpha_1,\alpha_2}\frac{\partial_z\phi_{n_{z_1}}\phi_{n_{z_2}} + \phi_{n_{z_1}}\partial_z\phi_{n_{z_2}}}{2}\phi^{|\Lambda_1|}_{n_{r_1}}\phi^{|\Lambda_2|}_{n_{r_2}}, \frac{\cos K\varphi}{2\pi},
\tag{E.6}
$$

$$
\delta f_\perp = \sum_{\substack{\alpha_1,\alpha_2\\ d_1=d_2\\ |\Lambda_1-\Lambda_2|=K}}\left(\frac{\delta\rho_1+\delta\rho_2}{2}\right)_{\alpha_1,\alpha_2}\phi_{n_{z_1}}\phi_{n_{z_2}}\frac{\partial_{r_\perp}\phi^{|\Lambda_1|}_{n_{r_1}}\phi^{|\Lambda_2|}_{n_{r_2}} + \phi^{|\Lambda_1|}_{n_{r_1}}\partial_{r_\perp}\phi^{|\Lambda_2|}_{n_{r_2}}}{2}\frac{\cos K\varphi}{2\pi},
\tag{E.7}
$$

we have:

$$
\begin{aligned}
\mathrm{Re}\left[\left\langle\sum_{\alpha_1,\alpha_2}\rho_{\alpha_1,\alpha_2}\langle\alpha_2; s|\overrightarrow{\nabla}|\alpha_1; s\rangle\right\rangle_{s=\pm\mathrm{i}}\right] &= \left(f_z^0 + 2\eta\,\mathrm{Re}\left[e^{-\mathrm{i}\omega t}\delta f_z\right] + \mathcal{O}(\eta^2)\right)\boldsymbol{e}_z \\
&+ \left(f_\perp^0 + 2\eta\,\mathrm{Re}\left[e^{-\mathrm{i}\omega t}\delta f_\perp\right] + \mathcal{O}(\eta^2)\right)\boldsymbol{e}_\perp \\
&+ \mathcal{O}(\eta)\boldsymbol{e}_\varphi.
\end{aligned}
\tag{E.8}
$$

Following analogous steps, but now for imaginary part, it is easy to see that the ground state part vanishes and we have:

$$\mathrm{Im}\left[\left\langle \sum_{\alpha_1,\alpha_2} \rho_{\alpha_1,\alpha_2} \langle \alpha_2; s| \overrightarrow{\nabla} |\alpha_1; s\rangle \right\rangle_{s=\pm \mathrm{i}}\right] = \mathcal{O}(\eta)\boldsymbol{e}_z + \mathcal{O}(\eta)\boldsymbol{e}_\perp + \mathcal{O}(\eta)\boldsymbol{e}_\varphi. \tag{E.9}$$

In total, when real and imaginary parts are combined, the second term in Eq. (70) is given by:

$$\begin{aligned}\left|\left\langle \sum_{\alpha_1,\alpha_2} \rho_{\alpha_1,\alpha_2} \langle \alpha_2; s| \overrightarrow{\nabla} |\alpha_1; s\rangle \right\rangle_{s=\pm \mathrm{i}}\right|^2 &= \left(f_z^0\right)^2 + \left(f_\perp^0\right)^2 \\ &+ 4\eta\,\mathrm{Re}\left[e^{-\mathrm{i}\omega t}\left(f_z^0 \delta f_z + f_\perp^0 \delta f_\perp\right)\right] + \mathcal{O}(\eta^2).\end{aligned} \tag{E.10}$$

Following the same steps, if we define:

$$g^0 = \sum_{\substack{\alpha_1,\alpha_2 \\ d_1=d_2 \\ |\Lambda_1-\Lambda_2|=0}} \mathrm{Re}[\rho_0]_{\alpha_1,\alpha_2} \phi_{n_{z_1}} \phi_{n_{z_2}} \phi_{n_{r_1}}^{|\Lambda_1|} \phi_{n_{r_2}}^{|\Lambda_2|} \frac{1}{2\pi}, \tag{E.11}$$

$$\begin{aligned}h^0 = \sum_{\substack{\alpha_1,\alpha_2 \\ d_1=d_2 \\ |\Lambda_1-\Lambda_2|=0}} \mathrm{Re}[\rho_0]_{\alpha_1,\alpha_2} \Big(&\partial_z \phi_{n_{z_1}} \partial_z \phi_{n_{z_2}} \phi_{n_{r_1}}^{|\Lambda_1|} \phi_{n_{r_2}}^{|\Lambda_2|} \\ &+ \phi_{n_{z_1}} \phi_{n_{z_2}} \partial_{r_\perp} \phi_{n_{r_1}}^{|\Lambda_1|} \partial_{r_\perp} \phi_{n_{r_2}}^{|\Lambda_2|} \\ &+ \phi_{n_{z_1}} \phi_{n_{z_2}} \phi_{n_{r_1}}^{|\Lambda_1|} \phi_{n_{r_2}}^{|\Lambda_2|} \frac{\Lambda_1 \Lambda_2}{r_\perp^2} \Big) \frac{1}{2\pi},\end{aligned} \tag{E.12}$$

$$\delta g = \sum_{\substack{\alpha_1,\alpha_2 \\ d_1=d_2 \\ |\Lambda_1-\Lambda_2|=K}} \left(\frac{\delta\rho_1 + \delta\rho_2}{2}\right)_{\alpha_1,\alpha_2} \phi_{n_{z_1}} \phi_{n_{z_2}} \phi_{n_{r_1}}^{|\Lambda_1|} \phi_{n_{r_2}}^{|\Lambda_2|} \frac{\cos K\varphi}{2\pi}, \tag{E.13}$$

$$\begin{aligned}\delta h = \sum_{\substack{\alpha_1,\alpha_2 \\ d_1=d_2 \\ |\Lambda_1-\Lambda_2|=K}} \left(\frac{\delta\rho_1 + \delta\rho_2}{2}\right)_{\alpha_1,\alpha_2} \Big(&\partial_z \phi_{n_{z_1}} \partial_z \phi_{n_{z_2}} \phi_{n_{r_1}}^{|\Lambda_1|} \phi_{n_{r_2}}^{|\Lambda_2|} \\ &+ \phi_{n_{z_1}} \phi_{n_{z_2}} \partial_{r_\perp} \phi_{n_{r_1}}^{|\Lambda_1|} \partial_{r_\perp} \phi_{n_{r_2}}^{|\Lambda_2|} \\ &+ \phi_{n_{z_1}} \phi_{n_{z_2}} \phi_{n_{r_1}}^{|\Lambda_1|} \phi_{n_{r_2}}^{|\Lambda_2|} \frac{\Lambda_1 \Lambda_2}{r_\perp^2} \Big) \frac{\cos K\varphi}{2\pi},\end{aligned} \tag{E.14}$$

the remaining parts needed to calculate D in Eq. (70) are given by:

$$\left\langle \sum_{\alpha_1,\alpha_2} \rho_{\alpha_1,\alpha_2} \langle \alpha_2; s|\alpha_1; s\rangle \right\rangle_{s=\pm \mathrm{i}} = g^0 + 2\eta\,\mathrm{Re}\left[e^{-\mathrm{i}\omega t}\delta g\right] + \mathcal{O}(\eta^2), \tag{E.15}$$

$$\left\langle \sum_{\alpha_1,\alpha_2} \rho_{\alpha_1,\alpha_2} \langle \alpha_2; s| \overleftarrow{\nabla}\overrightarrow{\nabla} |\alpha_1; s\rangle \right\rangle_{s=\pm \mathrm{i}} = h^0 + 2\eta\,\mathrm{Re}\left[e^{-\mathrm{i}\omega t}\delta h\right] + \mathcal{O}(\eta^2). \tag{E.16}$$

Next, we plug those parts into Eq. (70) and again keeping only the terms up to linear order in η parameter, we get:

$$D(\boldsymbol{x}, t) = D^0(\boldsymbol{x}) + 2\eta\,\mathrm{Re}\left[e^{-\mathrm{i}\omega t}\delta D(\boldsymbol{x}, \omega)\right] + \mathcal{O}(\eta^2), \tag{E.17}$$

where:

$$D^0(\boldsymbol{x}) = h^0(\boldsymbol{x}) - \frac{\left(f_z^0(\boldsymbol{x})\right)^2 + \left(f_\perp^0(\boldsymbol{x})\right)^2}{g^0(\boldsymbol{x})}, \tag{E.18}$$

$$\begin{aligned}\delta D(\boldsymbol{x}, \omega) = \delta h(\boldsymbol{x}, \omega) &+ \delta g(\boldsymbol{x}, \omega) \frac{\left(f_z^0(\boldsymbol{x})\right)^2 + \left(f_\perp^0(\boldsymbol{x})\right)^2}{\left(g^0(\boldsymbol{x})\right)^2} \\ &- 2\frac{f_z^0(\boldsymbol{x})\delta f_z(\boldsymbol{x}, \omega) + f_\perp^0(\boldsymbol{x})\delta f_\perp(\boldsymbol{x}, \omega)}{g^0(\boldsymbol{x})}.\end{aligned} \tag{E.19}$$

Next, the scaled $D(\boldsymbol{x}, t)$ with Thomas-Fermi density is:

$$\frac{D(\boldsymbol{x}, t)}{\tau_{\mathrm{TF}}(\boldsymbol{x})} = \underbrace{\frac{D^0(\boldsymbol{x}, t)}{\tau_{\mathrm{TF}}^0(\boldsymbol{x})}}_{F^0(\boldsymbol{x})} + 2\eta\,\mathrm{Re}\left[e^{-\mathrm{i}\omega t}\underbrace{\left(\frac{\delta D(\boldsymbol{x}, \omega)}{\tau_{\mathrm{TF}}^0(\boldsymbol{x})} - \frac{5}{3}\frac{D^0(\boldsymbol{x})}{\tau_{\mathrm{TF}}^0(\boldsymbol{x})}\frac{\delta g(\boldsymbol{x}, \omega)}{g^0(\boldsymbol{x})}\right)}_{\delta F(\boldsymbol{x}, \omega)}\right] + \mathcal{O}(\eta^2), \tag{E.20}$$

and finally, the nucleon localization function $\mathcal{C}(\boldsymbol{x},t)$ is:

$$\mathcal{C}(\boldsymbol{x},t)=\underbrace{\frac{1}{1+\left(F^0(\boldsymbol{x})\right)^2}}_{\mathcal{C}^0(\boldsymbol{x})}+2\eta\,\mathrm{Re}\left[e^{-\mathrm{i}\omega t}\underbrace{\left(\frac{-2F^0(\boldsymbol{x})\delta F(\boldsymbol{x},\omega)}{\left(1+\left(F^0(\boldsymbol{x})\right)^2\right)^2}\right)}_{\delta\mathcal{C}(\boldsymbol{x},\omega)}\right]+\mathcal{O}(\eta^2). \tag{E.21}$$

Appendix F. Elimination of the translational spurious mode

For completeness, here we describe the implementation of the method for elimination of the translational spurious mode [22]. The phonon operator is given by:

$$\hat{O}^\dagger=\frac{1}{2}\sum_{\mu,\nu}X_{\mu\nu}\hat{\alpha}^\dagger_\mu\hat{\alpha}^\dagger_\nu-Y_{\mu\nu}\hat{\alpha}_\nu\hat{\alpha}_\mu, \tag{F.1}$$

while the center of mass and total momentum operators in quasiparticle basis read:

$$\hat{R}=\frac{1}{2}\sum_{\mu,\nu}R^{20}_{\mu\nu}\hat{\alpha}^\dagger_\mu\hat{\alpha}^\dagger_\nu+R^{02}_{\mu\nu}\hat{\alpha}_\nu\hat{\alpha}_\mu, \tag{F.2}$$

$$\hat{P}=\frac{1}{2}\sum_{\mu,\nu}P^{20}_{\mu\nu}\hat{\alpha}^\dagger_\mu\hat{\alpha}^\dagger_\nu+P^{02}_{\mu\nu}\hat{\alpha}_\nu\hat{\alpha}_\mu. \tag{F.3}$$

Because the operators α_μ and α_ν anticommute, the X and Y matrices are antisymmetric: $X^T=-X$ and $Y^T=-Y$. Furthermore, since the operators $\hat{R}$ and $\hat{P}$ are Hermitian, the following relations hold: $R^{02}=\left(R^{20}\right)^*$, $P^{02}=\left(P^{20}\right)^*$. The self-consistent solution $\hat{O}^\dagger_{(\mathrm{calc})}$ contains both the physical solution $\hat{O}^\dagger_{(\mathrm{phys})}$ as well as the admixtures of the spurious modes:

$$\hat{O}^\dagger_{(\mathrm{calc})}=\hat{O}^\dagger_{(\mathrm{phys})}+\lambda_R\hat{R}+\lambda_P\hat{P}. \tag{F.4}$$

Since the physical modes should be orthogonal to the spurious mode, we require:

$$\langle\Phi|\left[\hat{O}^\dagger_{(\mathrm{phys})},\hat{R}\right]|\Phi\rangle=0\quad\text{and}\quad\langle\Phi|\left[\hat{O}^\dagger_{(\mathrm{phys})},\hat{P}\right]|\Phi\rangle=0. \tag{F.5}$$

Previous equations allow us to calculate the λ_R and λ_P coefficients:

$$\lambda_R=+\frac{\langle\Phi|\left[\hat{O}^\dagger_{(\mathrm{calc})},\hat{P}\right]|\Phi\rangle}{\langle\Phi|\left[\hat{R},\hat{P}\right]|\Phi\rangle}\quad\text{and}\quad\lambda_P=-\frac{\langle\Phi|\left[\hat{O}^\dagger_{(\mathrm{calc})},\hat{R}\right]|\Phi\rangle}{\langle\Phi|\left[\hat{R},\hat{P}\right]|\Phi\rangle}. \tag{F.6}$$

Using the anticommutation relation $\left\{\alpha^\dagger_\mu,\alpha_\nu\right\}=\delta_{\mu\nu}$, one can easily evaluate:

$$\langle\Phi|\left[\hat{O}^\dagger_{(\mathrm{calc})},\hat{R}\right]|\Phi\rangle=\frac{1}{2}\mathrm{Tr}\left[X^{(\mathrm{calc})}\left(R^{20}\right)^*+Y^{(\mathrm{calc})}R^{20}\right], \tag{F.7}$$

$$\langle\Phi|\left[\hat{O}^\dagger_{(\mathrm{calc})},\hat{P}\right]|\Phi\rangle=\frac{1}{2}\mathrm{Tr}\left[X^{(\mathrm{calc})}\left(P^{20}\right)^*+Y^{(\mathrm{calc})}P^{20}\right], \tag{F.8}$$

$$\langle\Phi|\left[\hat{R},\hat{P}\right]|\Phi\rangle=\mathrm{i}\,\mathrm{Im}\left[\mathrm{Tr}\left[(R^{20})^\dagger\frac{1}{2}\left(P^{20}-\left(P^{20}\right)^T\right)\right]\right]. \tag{F.9}$$

Notice that if we used a complete harmonic oscillator basis, the following relation would hold: $\langle\Phi|\left[\hat{R},\hat{P}\right]|\Phi\rangle=\mathrm{i}$. However, in practical calculations harmonic oscillator basis is truncated which yields a correction term in Eq. (F.9). Of course, as one increases the number of oscillator shells in the basis, the value of $\langle\Phi|\left[\hat{R},\hat{P}\right]|\Phi\rangle$ approaches i. Once the scalars λ_R and λ_P are evaluated, Eq. (F.4) yields the corrected values for QFAM amplitudes:

$$X^{(\mathrm{phys})}_{\mu\nu}=X^{(\mathrm{calc})}_{\mu\nu}-\lambda_R R^{20}_{\mu\nu}-\lambda_P P^{20}_{\mu\nu}, \tag{F.10}$$

$$Y^{(\mathrm{phys})}_{\mu\nu}=Y^{(\mathrm{calc})}_{\mu\nu}+\lambda_R\left(R^{20}_{\mu\nu}\right)^*+\lambda_P\left(P^{20}_{\mu\nu}\right)^*. \tag{F.11}$$

We now focus on the specific operators in the simplex-y HO basis used within the `DIRQFAM` code. The excitation operator is given by:

$$\hat{f}^{(+)}_{JK}=\frac{\hat{f}_{J,K}+(-1)^K\hat{f}_{J,-K}}{\sqrt{2+2\delta_{K,0}}}, \tag{F.12}$$

where:

$$\hat{f}_{J,K} = \sum_{p=1}^{Z} |\boldsymbol{r}^{(p)}|^J Y_{J,K}(\theta^{(p)}, \varphi^{(p)}) \pm \sum_{n=1}^{N} |\boldsymbol{r}^{(n)}|^J Y_{J,K}(\theta^{(n)}, \varphi^{(n)}). \tag{F.13}$$

The center of mass operator $\hat{R}^K_{\mathrm{CM}}$ is given by:

$$\hat{R}^K_{\mathrm{CM}} = \frac{1}{A} \sum_{i=1}^{A} \boldsymbol{r}^{(i)}_{1,K}, \tag{F.14}$$

with:

$$\boldsymbol{r}_{1,+1} = \frac{+1}{\sqrt{2}} r_\perp e^{-\mathrm{i}\varphi}, \quad \boldsymbol{r}_{1,0} = z, \quad \boldsymbol{r}_{1,-1} = \frac{-1}{\sqrt{2}} r_\perp e^{+\mathrm{i}\varphi}. \tag{F.15}$$

However, because the operator $\hat{f}^{(+)}_{J,K}$ excites both $+K$ and $-K$ modes, we have to make an analogous adjustment as in Eq. (F.12). For $K = 0$ the operator $\hat{R}^{K=0}_{\mathrm{CM}}$ remains unmodified:

$$\hat{R}^{K=0}_{\mathrm{CM}} = \frac{1}{A} \sum_{i=1}^{A} z^{(i)}, \tag{F.16}$$

while for $K = 1$ we define the operator:

$$\hat{R}^{K=1}_{\mathrm{CM}} = \frac{1}{A} \sum_{i=1}^{A} r^{(i)}_\perp \cos\varphi^{(i)} = \frac{1}{A} \sum_{i=1}^{A} x^{(i)}. \tag{F.17}$$

The corresponding total momentum operators are given by:

$$\hat{P}^{K=0}_{\mathrm{CM}} = -\mathrm{i} \sum_{i=1}^{A} \partial_{z^{(i)}}, \tag{F.18}$$

$$\hat{P}^{K=1}_{\mathrm{CM}} = -\mathrm{i} \sum_{i=1}^{A} \partial_{x^{(i)}} = -\mathrm{i} \sum_{i=1}^{A} \cos\varphi^{(i)} \partial_{r^{(i)}_\perp} - \frac{\sin\varphi^{(i)}}{r^{(i)}_\perp} \partial_{\varphi^{(i)}}. \tag{F.19}$$

Next we calculate the matrix representations of operators $\hat{R}^K_{\mathrm{CM}}$ and $\hat{P}^K_{\mathrm{CM}}$ in the simplex-y HO basis. We use the same notation as in Appendix E. One can easily prove the following relations:

$$\langle \alpha_1, s_1 | \hat{R}^{K=0}_{\mathrm{CM}} | \alpha_2, s_2 \rangle = \frac{1}{A} \delta_{s_1,s_2} \delta_{d_1,d_2} \delta_{n_{r_1},n_{r_2}} \delta_{|\Lambda_1-\Lambda_2|,0} \int_{-\infty}^{+\infty} z \phi_{n_{z_1}} \phi_{n_{z_2}} dz, \tag{F.20}$$

$$\begin{aligned} \langle \alpha_1, s_1 | \hat{P}^{K=0}_{\mathrm{CM}} | \alpha_2, s_2 \rangle = {} & \frac{-\mathrm{i}}{2} \delta_{s_1,s_2} \delta_{d_1,d_2} \delta_{n_{r_1},n_{r_2}} \delta_{|\Lambda_1-\Lambda_2|,0} \times \\ & \times \int_{-\infty}^{+\infty} \left(\phi_{n_{z_1}} \partial_z \phi_{n_{z_2}} - \phi_{n_{z_2}} \partial_z \phi_{n_{z_1}} \right) dz, \end{aligned} \tag{F.21}$$

$$\langle \alpha_1, s_1 | \hat{R}^{K=1}_{\mathrm{CM}} | \alpha_2, s_2 \rangle = \frac{1}{2A} \delta_{s_1,s_2} \delta_{d_1,d_2} \delta_{n_{z_1},n_{z_2}} \delta_{|\Lambda_1-\Lambda_2|,1} \int_{0}^{+\infty} r_\perp \phi^{|\Lambda_1|}_{n_{r_1}} \phi^{|\Lambda_2|}_{n_{r_2}} r_\perp dr_\perp, \tag{F.22}$$

$$\begin{aligned} \langle \alpha_1, s_1 | \hat{P}^{K=1}_{\mathrm{CM}} | \alpha_2, s_2 \rangle = {} & \frac{-\mathrm{i}}{4} \delta_{s_1,s_2} \delta_{d_1,d_2} \delta_{n_{z_1},n_{z_2}} \delta_{|\Lambda_1-\Lambda_2|,1} \times \\ \times \int_{0}^{+\infty} & \left[\left(\phi^{|\Lambda_1|}_{n_{r_1}} \partial_{r_\perp} \phi^{|\Lambda_2|}_{n_{r_2}} - \phi^{|\Lambda_2|}_{n_{r_2}} \partial_{r_\perp} \phi^{|\Lambda_1|}_{n_{r_1}} \right) + \frac{\Lambda_2^2 - \Lambda_1^2}{r_\perp} \phi^{|\Lambda_1|}_{n_{r_1}} \phi^{|\Lambda_2|}_{n_{r_2}} \right] r_\perp dr_\perp. \end{aligned} \tag{F.23}$$

Previous equations show that the matrices R_{CM} and P_{CM} are block diagonal in the simplex-y HO basis:

$$R_{\mathrm{CM}} = \begin{bmatrix} r_{\mathrm{CM}} & 0 \\ 0 & r_{\mathrm{CM}} \end{bmatrix} \quad \text{and} \quad P_{\mathrm{CM}} = \begin{bmatrix} p_{\mathrm{CM}} & 0 \\ 0 & p_{\mathrm{CM}} \end{bmatrix}, \tag{F.24}$$

where Hermitian matrix r_{CM} satisfies $r_{\mathrm{CM}} = r^*_{\mathrm{CM}} = r^T_{\mathrm{CM}}$ and Hermitian matrix p_{CM} satisfies $p_{\mathrm{CM}} = -p^*_{\mathrm{CM}} = -p^T_{\mathrm{CM}}$. Matrices r_{CM} and p_{CM} can easily be calculated by using Eqs. (F.20)-(F.23) thus yielding the matrices R^{20} and P^{20}:

$$R^{20} = \begin{bmatrix} 0 & r^{20} \\ -\left(r^{20}\right)^T & 0 \end{bmatrix} \quad \text{and} \quad P^{20} = \begin{bmatrix} 0 & p^{20} \\ -\left(p^{20}\right)^T & 0 \end{bmatrix}. \tag{F.25}$$

Matrices r^{20} and p^{20} read[7]:

$$r^{20} = -\left(u^{\dagger} r_{\mathrm{CM}} v + v^{\dagger} r_{\mathrm{CM}}^{T} u\right) \quad \text{and} \quad p^{20} = -\left(u^{\dagger} p_{\mathrm{CM}} v + v^{\dagger} p_{\mathrm{CM}}^{T} u\right). \tag{F.26}$$

The general expression for the expectation value $\langle\Phi|\left[\hat{R}, \hat{P}\right]|\Phi\rangle$ in Eq. (F.9) can be written as:

$$\langle\Phi|\left[\hat{R}, \hat{P}\right]|\Phi\rangle = 2\,\mathrm{Tr}\left[\left(r^{20}\right)^{\dagger} p^{20}\right]. \tag{F.27}$$

Using the block simplex form of the X and Y matrices:

$$X = \begin{bmatrix} 0 & x \\ -x^{T} & 0 \end{bmatrix} \quad \text{and} \quad Y = \begin{bmatrix} 0 & y \\ -y^{T} & 0 \end{bmatrix}, \tag{F.28}$$

we obtain the following expressions for the expectation values $\langle\Phi|\left[\hat{O}^{\dagger}_{(\mathrm{calc})}, \hat{R}\right]|\Phi\rangle$ and $\langle\Phi|\left[\hat{O}^{\dagger}_{(\mathrm{calc})}, \hat{P}\right]|\Phi\rangle$ in Eqs. (F.7) and (F.8):

$$\langle\Phi|\left[\hat{O}^{\dagger}_{(\mathrm{calc})}, \hat{R}\right]|\Phi\rangle = -\,\mathrm{Tr}\left[\left(r^{20}\right)^{\dagger}\left(+x + y^{T}\right)\right], \tag{F.29}$$

$$\langle\Phi|\left[\hat{O}^{\dagger}_{(\mathrm{calc})}, \hat{P}\right]|\Phi\rangle = +\,\mathrm{Tr}\left[\left(p^{20}\right)^{\dagger}\left(-x + y^{T}\right)\right]. \tag{F.30}$$

Equations (F.10) and (F.11), providing the spurious free values for the QFAM amplitudes, read:

$$x^{(\mathrm{phys})}_{\mu\nu} = x^{(\mathrm{calc})}_{\mu\nu} - \lambda_R r^{20}_{\mu\nu} - \lambda_P p^{20}_{\mu\nu}, \tag{F.31}$$

$$y^{(\mathrm{phys})}_{\mu\nu} = y^{(\mathrm{calc})}_{\mu\nu} + \lambda_R \left(r^{20}_{\mu\nu}\right)^{*} + \lambda_P \left(p^{20}_{\mu\nu}\right)^{*}. \tag{F.32}$$

To summarize, if the excitation operator has an odd value of J and K is equal to 0 or 1, the response is contaminated by the spurious $K^{\pi} = 0^{-}$ or $K^{\pi} = 1^{-}$ contributions. Once the self-consistent solution $x^{(\mathrm{calc})}(\omega)$, $y^{(\mathrm{calc})}(\omega)$ is found, we first calculate the scalar coefficients:

$$\lambda_R = \frac{\mathrm{Tr}\left[\left(p^{20}\right)^{\dagger}\left(-x^{(\mathrm{calc})}(\omega) + y^{(\mathrm{calc})}(\omega)^{T}\right)\right]}{\langle\Phi|\left[\hat{R}, \hat{P}\right]|\Phi\rangle}, \tag{F.33}$$

$$\lambda_P = \frac{\mathrm{Tr}\left[\left(r^{20}\right)^{\dagger}\left(+x^{(\mathrm{calc})}(\omega) + y^{(\mathrm{calc})}(\omega)^{T}\right)\right]}{\langle\Phi|\left[\hat{R}, \hat{P}\right]|\Phi\rangle}. \tag{F.34}$$

Notice that both expressions in the numerator and denominator have to be summed over both the proton and the neutron contribution. Next, we calculate the corrected values of the QFAM amplitudes $x^{(\mathrm{phys})}(\omega)$ and $y^{(\mathrm{phys})}(\omega)$ according to Eqs. (F.31) and (F.32). Finally, these corrected values are used to calculate the spurious mode free response function. We have verified that for the isoscalar $J = 1$ and $K = 0, 1$ excitation operator Eq. (F.12), the calculated response after correction is precisely zero.

References

[1] A. Bjelčić, T. Nikšić, Comput. Phys. Commun. 253 (2020) 107184.
[2] P. Ring, Prog. Part. Nucl. Phys. 37 (1996) 193.
[3] S. Typel, H.H. Wolter, Nucl. Phys. A 656 (1999) 331.
[4] F. Hofmann, C.M. Keil, H. Lenske, Phys. Rev. C 64 (2001) 034314.
[5] T. Niksic, D. Vretenar, P. Finelli, P. Ring, Phys. Rev. C 66 (2002) 024306.
[6] G.A. Lalazissis, T. Nikšić, D. Vretenar, P. Ring, Phys. Rev. C 71 (2005) 024312.
[7] C.W. Johnson, G.F. Bertsch, W.D. Hazelton, Comput. Phys. Commun. 120 (1999) 155.
[8] J. Toivanen, B.G. Carlsson, J. Dobaczewski, K. Mizuyama, R.R. Rodríguez-Guzmán, P. Toivanen, P. Veselý, Phys. Rev. C 81 (2010) 034312.
[9] B.G. Carlsson, J. Toivanen, A. Pastore, Phys. Rev. C 86 (2012) 014307.
[10] Y. Saad, Iterative Methods for Sparse Linear Systems, 2nd edition, SIAM, 2003.
[11] A. Baran, A. Bulgac, M. McNeil Forbes, G. Hagen, W. Nazarewicz, N. Schunck, M. Stoitsov, Phys. Rev. C 78 (2008) 014318.
[12] Y. Tian, Z.Y. Ma, P. Ring, Phys. Rev. C 79 (2009) 064301.
[13] Y. Tian, Z.Y. Ma, P. Ring, Phys. Rev. C 80 (2009) 024313.
[14] A.D. Becke, K.E. Edgecombe, J. Chem. Phys. 92 (1990) 5397.
[15] P.-G. Reinhard, J.A. Maruhn, A.S. Umar, V.E. Oberacker, Phys. Rev. C 83 (2011) 034312.
[16] P. Ring, P. Schuck, The Nuclear Many-Body Problem, Springer-Verlag, Berlin, 1980.
[17] N. Hinohara, M. Kortelainen, W. Nazarewicz, Phys. Rev. C 87 (2013) 064309.
[18] N. Paar, D. Vretenar, E. Khan, G. Colo, Rep. Prog. Phys. 70 (2007) 691.
[19] Y. Zhan, A. Bjelčić, T. Nikšić, E. Litvinova, P. Ring, P. Schuck, Phys. Rev. C 105 (2022) 044326.
[20] T. Nikšić, N. Paar, D. Vretenar, P. Ring, Comput. Phys. Commun. 185 (2014) 1808.
[21] D. Vautherin, Phys. Rev. C 7 (1973) 296.
[22] T. Nakatsukasa, T. Inakura, K. Yabana, Phys. Rev. C 76 (2007) 024318.

[7] See Eq. (B.6) in Ref. [1].